Optimization of a high-yield, low-areal-density fusion product source at the National Ignition Facility with applications in nucleosynthesis experiments

M. Gatu Johnson, D. T. Casey, M. Hohenberger, A. B. Zylstra, A. Bacher, C. R. Brune, R. M. Bionta, R. S. Craxton, C. L. Ellison, M. Farrell, J. A. Frenje, W. Garbett, E. M. Garcia, G. P. Grim, E. Hartouni, R. Hatarik, H. W. Herrmann, M. Hohensee, D. M. Holunga, M. Hoppe, M. Jackson, N. Kabadi, S. F. Khan, J. D. Kilkenny, T. R. Kohut, B. Lahmann, H. P. Le, C. K. Li, L. Masse, P. W. McKenty, D. P. McNabb, A. Nikroo, T. G. Parham, C. E. Parker, R. D. Petrasso, J. Pino, B. Remington, N. G. Rice, H. G. Rinderknecht, M. J. Rosenberg, J. Sanchez, D. B. Sayre, M. E. Schoff, C. M. Shuldberg, F. H. Séguin, H. Sio, Z. B. Walters, and H. D. Whitley

Citation: Physics of Plasmas **25**, 056303 (2018); doi: 10.1063/1.5017746

View online: https://doi.org/10.1063/1.5017746

View Table of Contents: http://aip.scitation.org/toc/php/25/5

Published by the American Institute of Physics

Optimization of a high-yield, low-areal-density fusion product source at the National Ignition Facility with applications in nucleosynthesis experiments

M. Gatu Johnson,[1,a)] D. T. Casey,[2] M. Hohenberger,[2] A. B. Zylstra,[3] A. Bacher,[4] C. R. Brune,[5] R. M. Bionta,[2] R. S. Craxton,[6] C. L. Ellison,[2] M. Farrell,[7] J. A. Frenje,[1] W. Garbett,[8] E. M. Garcia,[6] G. P. Grim,[2] E. Hartouni,[2] R. Hatarik,[2] H. W. Herrmann,[3] M. Hohensee,[2] D. M. Holunga,[2] M. Hoppe,[7] M. Jackson,[7] N. Kabadi,[1] S. F. Khan,[2] J. D. Kilkenny,[7] T. R. Kohut,[2] B. Lahmann,[1] H. P. Le,[2] C. K. Li,[1] L. Masse,[2] P. W. McKenty,[6] D. P. McNabb,[2] A. Nikroo,[2] T. G. Parham,[2] C. E. Parker,[1] R. D. Petrasso,[1] J. Pino,[2] B. Remington,[2] N. G. Rice,[7] H. G. Rinderknecht,[2] M. J. Rosenberg,[6] J. Sanchez,[2] D. B. Sayre,[2] M. E. Schoff,[7] C. M. Shuldberg,[7] F. H. Séguin,[1] H. Sio,[1] Z. B. Walters,[2] and H. D. Whitley[2]

[1]*Massachusetts Institute of Technology, Plasma Science and Fusion Center, Cambridge, Massachusetts 02139, USA*
[2]*Lawrence Livermore National Laboratory, Livermore, California 94550, USA*
[3]*Los Alamos National Laboratory, Los Alamos, New Mexico 87544, USA*
[4]*Department of Physics, Indiana University, Bloomington, Indiana 47405, USA*
[5]*Department of Physics and Astronomy, Ohio University, Athens, Ohio 45701, USA*
[6]*Laboratory for Laser Energetics, University of Rochester, Rochester, New York 14623, USA*
[7]*General Atomics, San Diego, California 92186, USA*
[8]*AWE plc, Aldermaston, Reading RG7 4PR, United Kingdom*

(Received 29 November 2017; accepted 2 February 2018; published online 9 March 2018)

Polar-direct-drive exploding pushers are used as a high-yield, low-areal-density fusion product source at the National Ignition Facility with applications including diagnostic calibration, nuclear security, backlighting, electron-ion equilibration, and nucleosynthesis-relevant experiments. In this paper, two different paths to improving the performance of this platform are explored: (i) optimizing the laser drive, and (ii) optimizing the target. While the present study is specifically geared towards nucleosynthesis experiments, the results are generally applicable. Example data from T_2/^{3}He-gas-filled implosions with trace deuterium are used to show that yield and ion temperature (T_{ion}) from 1.6 mm-outer-diameter thin-glass-shell capsule implosions are improved at a set laser energy by switching from a ramped to a square laser pulse shape, and that increased laser energy further improves yield and T_{ion}, although by factors lower than predicted by 1 D simulations. Using data from D_2/^{3}He-gas-filled implosions, yield at a set T_{ion} is experimentally verified to increase with capsule size. Uniform D^{3}He-proton spectra from 3 mm-outer-diameter CH shell implosions demonstrate the utility of this platform for studying charged-particle-producing reactions relevant to stellar nucleosynthesis. *Published by AIP Publishing.* https://doi.org/10.1063/1.5017746

I. INTRODUCTION

A low-areal-density, high-yield "exploding pusher" implosion platform was initially developed at the National Ignition Facility[1] (NIF) for nuclear diagnostic calibration purposes.[2,3] This platform has been subsequently adapted to serve as a mono-energetic fusion product source for use in charged-particle backlighting experiments.[4] It has also been used to study ion-kinetic effects in inertial confinement fusion (ICF) implosions.[5] In parallel, a similar platform was also developed with the initial goal of studying ion-electron equilibration on the NIF.[6,7] These low-areal-density, high-yield implosions are useful for a variety of applications, including the already mentioned diagnostic calibration, backlighting, and ion-electron equilibration experiments, but also, e.g., as a neutron source for nuclear security-relevant applications (a recent DT-gas-filled variant obtained the highest recorded yield from a non-cryogenic capsule). The present paper focuses on the use and optimization of this platform for experiments probing nucleosynthesis-relevant charged-particle-producing nuclear reactions such as ^{3}He(^{3}He,2p)α. However, lessons from this work will also inform future optimization of the platform for other applications.

ICF implosions provide an interesting platform for studying nucleosynthesis-relevant nuclear reactions because they allow for temperature, density, reactant distribution, and screening conditions found in stars to be closely replicated in the laboratory.[8,9] In this sense, the ICF platform provides a valuable complement to accelerator experiments traditionally used to explore these reactions.[10] Initial experiments to probe stellar[11] and big-bang[12] nucleosynthesis-relevant reactions using the ICF platform took place at the OMEGA laser facility.[13] ^{3}He(^{3}He,2p)α is of particular interest because of its role as the primary energy-producing step in the solar proton-proton-I (pp-I) chain.[14] The reactivity of the ^{3}He(^{3}He,2p)α reaction determines the branching ratio pp-I/(pp-II + pp-III) in the sun, and accurate knowledge of this reactivity is important for better constraining neutrino oscillation parameters.[14] In addition, this 6-nucleon reaction with

Note: Paper TI3 5, Bull. Am. Phys. Soc. **62**, 314 (2017).
[a)]Invited speaker.

three particles in the final stage is very complicated to calculate theoretically. Measurements of the shape of the resulting proton energy spectrum will inform basic nuclear physics calculations and may also impact inference of the ^{3}He(^{3}He,2p)α reactivity from accelerator measurements (the analysis of these measurements[15,16] assumes an elliptical shape of the proton spectrum,[16] a shape which we now believe is incorrect[11]). The ^{3}He(^{3}He,2p)α proton spectrum has recently been measured at OMEGA at a center-of-mass energy ($E_{c.m.}$) of 165 keV (T_{ion} = 27 keV).[11] In the sun, this reaction takes place at $E_{c.m.}$= 22 keV (T_{ion} = 1.3 keV). The goal of the NIF ^{3}He(^{3}He,2p)α experiments is to bridge the gap between OMEGA and the sun, pushing the boundaries towards more stellar-relevant energies. (This has become even more interesting after recent measurements of the mirror T(t,2n)α reaction demonstrated a change in shape of the neutron energy spectrum over the relatively narrow $E_{c.m.}$ range 16–50 keV.[17]) The laser energy and power available on the NIF (max 1.8 MJ, 500 TW) are much higher than at OMEGA (max 30 kJ, 30 TW). This allows NIF to generate larger plasma volumes compared to OMEGA, which enables experiments with equivalent yield, and thus similar data quality, at lower plasma ion temperature (T_{ion}) and, hence, conditions more directly relevant to stellar nucleosynthesis.[9] A challenge in this context is that the NIF beam geometry is optimized for indirect drive using a hohlraum, while direct drive is required for these experiments because the combined charged-particle energy loss in the plasma and hohlraum would be unacceptably high. The 192 laser beams are organized into two inner (23.5° and 30°) and two outer (44.5° and 50°) upper and lower cones [Fig. 1(a)], which means that directly driven implosions on the NIF are restricted to polar-direct-drive (PDD) geometries.[18–20] Symmetry in polar-direct drive is optimized by varying the pointing of the beams onto the target[9] and/or the relative energy between the beams.[6] When the relative energy is varied, this is typically done by changing the "cone fraction," i.e., the fraction of the total energy in the inner beams [green in Fig. 1(a)].

Initial attempts to use the NIF low-areal-density, high-yield fusion product source for nucleosynthesis-relevant experiments were described in Ref. 9. Studying charged-particle-producing nucleosynthesis-relevant reactions requires low areal density and high yield (for the ^{3}He(^{3}He,2p)α reaction, we aim for $\rho R < 10$ mg/cm^2 and yield $> 10^7$), and further development was required to optimize the platform for these measurements. This paper describes two avenues pursued to improve performance for these experiments as well as for other experiments utilizing a similar platform: (i) optimizing the laser drive and (ii) optimizing the target. The results clearly demonstrate that 1.6 mm-outer-diameter (OD) thin-glass-shell capsules [Fig. 1(b] are more effectively driven with a square laser pulse than with a ramped pulse at equivalent energy, and that higher power can be used to achieve higher-T_{ion}, higher-yield, lower-ρR implosions (Sec. II). It is also experimentally verified that higher yield at equivalent T_{ion} can be obtained by using larger capsules; specifically, we compare results from 1.6 mm-OD SiO_2-shell capsules [Fig. 1(b)] and 3 mm-OD CH-shell capsules [Fig. 1(c)] (Sec. III). (The material switch is because of target fabrication considerations - SiO_2-shell technology is currently limited to ~2.1 mm maximum diameter.) Note that neither of the experiments described in the present paper utilizes the full energy available on the NIF (although still more than available on any other laser facility in the world). The simple reason for this is that to ensure success of the experiments, we did not want to immediately venture too far from platforms that had been previously tried. This obviously means that there is still headroom to push to even larger capsules and thus even lower T_{ion} at equivalent yield (see discussion at the end of Sec. III).

The paper is organized as follows: Section II describes how the implosions can be optimized by tuning the laser drive for 1.6 mm-OD SiO_2 shell implosions, Sec. III discusses optimizing the implosions by going to larger capsules, and Sec. IV concludes the paper.

II. OPTIMIZING THE LASER DRIVE

Initial experiments to study the stellar-relevant ^{3}He(^{3}He,2p)α reaction and the complementary T(T,2n)α and T(^{3}He,np)α reactions using exploding pusher implosions at the NIF demonstrated promising performance in terms of symmetry of emitted charged particle yields and spectra and reasonably low areal density, but generated a ^{3}He^{3}He-proton yield too low for accurate study of this reaction (minimum required yield ~10^7, achieved yield 4×10^5).[9] The yield was lower than expected, and this was attributed to lower than predicted T_{ion} (~6 keV achieved vs 11 keV predicted) for these ^{3}He-gas-filled, 1.6 mm-outer-diameter, 4.7–μm wall-thickness SiO_2 capsules shot with a 113-kJ, 2.1-ns-long ramped laser pulse. As a first step towards achieving high enough yields, it was decided to increase the laser power and/or energy delivered to the capsules in an attempt to increase T_{ion}. Ares[21,22] and HYDRA[23] simulations undertaken to optimize the drive indicated that the capsules would be more effectively driven with a square than a ramped laser pulse; in particular, the HYDRA simulations predicted lower

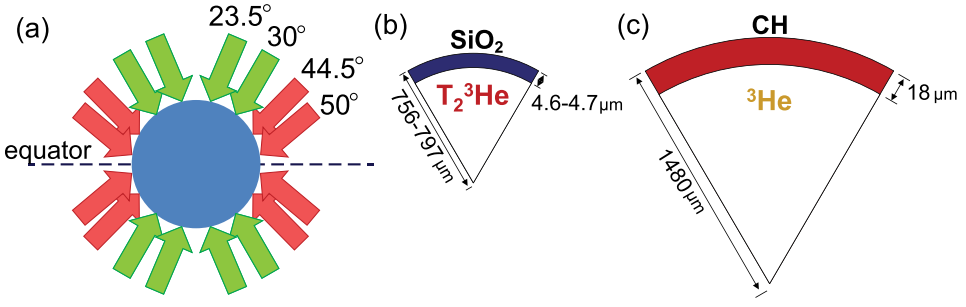

FIG. 1. (a) Laser drive geometry, (b) SiO_2 shell capsule, and (c) CH shell capsule used in the shock-driven "exploding pusher" experiments discussed in this paper. On the NIF, the beam configuration with the 192 beams configured in 2 inner (green, 23.5° and 30°) and 2 outer (red, 44.5° and 50°) cones restricts the laser drive to polar-direct-drive geometry.

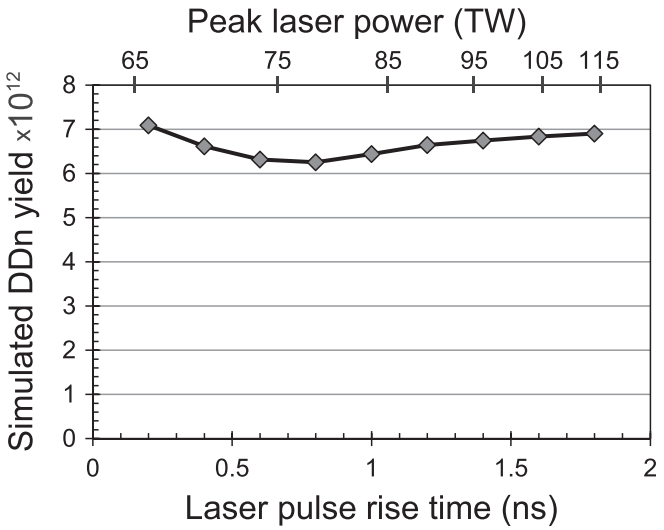

FIG. 2. Simulated DD-neutron yield vs laser pulse rise time from 1 D Ares simulations with a 2.0-ns duration, 125-kJ laser pulse incident on a 4-μm thick, 1.6-mm outer diameter SiO_2 shell filled with 3.3 atm D_2 gas. Since the laser energy and pulse duration are kept fixed in this scan, peak laser power is reduced with shorter rise time (upper scale).

ρR for the square pulse drive. Figure 2 shows the 1 D Ares-simulated DD-neutron yield as a function of laser-pulse rise time for a 2.0-ns duration, 125-kJ laser pulse incident on a 4–μm-thick, 1.6-mm outer-diameter SiO_2 shell filled with 3.3 atm D_2 gas. This scan predicts a minimal impact on yield from changing the laser pulse rise time (hence shape) at fixed energy and laser pulse duration. However, note that with the fixed energy and pulse duration, the peak laser power is reduced with shorter rise time. A shorter, higher-power square pulse with the same total energy is expected to give better performance than a longer, lower-power square pulse.

A square-pulse 1 D-Ares laser power/pulse duration scan (Fig. 3) was run in an effort to determine the optimal drive conditions for maximal yield at minimal T_{ion} with acceptable ρR. This scan, which spanned absorbed[24] laser powers from 27 to 162 TW and pulse durations from 0.6–2 ns, was done for 1.51 mm-OD, 4.7 μm-wall SiO_2 capsules filled with 5.15 atm tritium, 0.05 atm deuterium, and 2.6 atm ^{3}He. The yield, T_{ion}, bang-time, and ρR results shown in Fig. 3 come from a free-fall analysis[25] of the 1 D-Ares simulations. (The free-fall analysis, which artificially truncates yield generated at late times in the simulations, is intended to compensate for effects of hydrodynamic instability growth and shell-fuel mixing leading to a decrease in yield for these PDD implosions. An alternative to the free-fall analysis is to use molecular diffusion multipliers to enhance mix; this approach was taken for the simulations described in Ref. 6.) The simulations indicate that T_{ion} can be expected to increase monotonically with power over the range studied [Fig. 3(b)], while yield only increases up to a point [note the roll-over for absorbed powers higher than 81 TW, Fig. 3(a)]. Predicted total ρRs are acceptably low ($<$10 mg/cm^2) for absorbed power $>$81 TW [Fig. 3(d)]. Not surprisingly, bang time also drops monotonically with power [Fig. 3(c)]. It has been demonstrated that bang time after the end of the laser pulse is advantageous for charged-particle measurements to avoid both charged-particle yield asymmetries[26] and energy upshifts[27,28] due to capsule charging, so attempting to balance pulse duration to achieve bang time after the end of the laser pulse [dashed line in Fig. 3(c)] is a

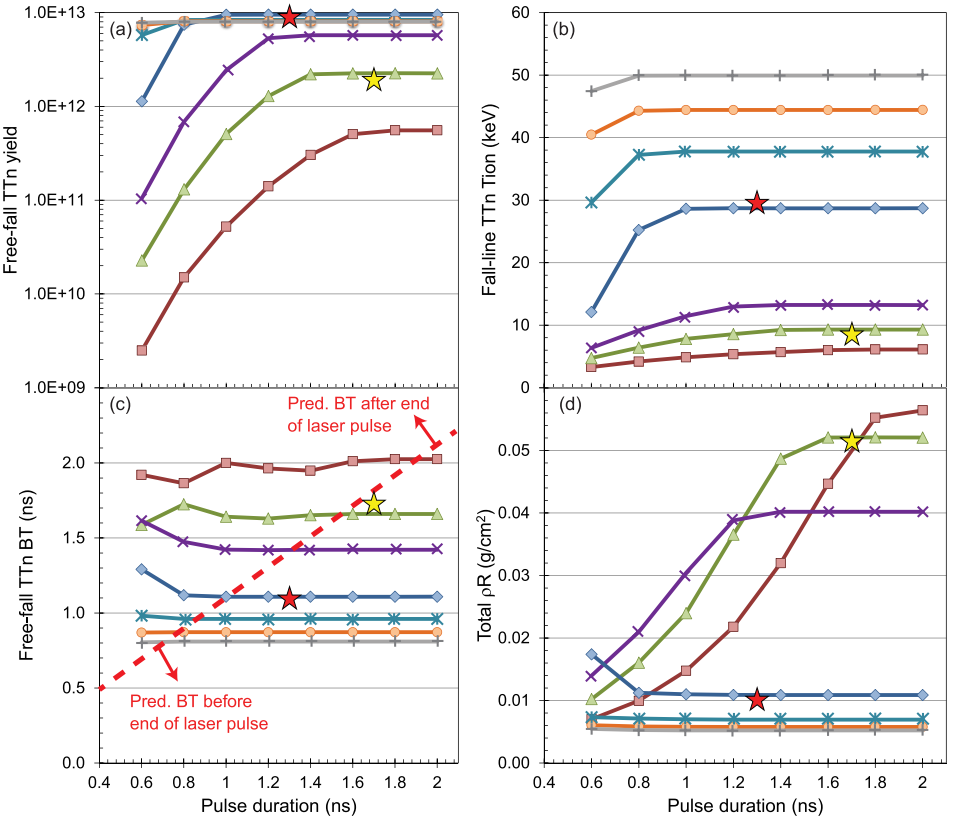

FIG. 3. TT-n (a) yield, (b) T_{ion}, (c) bang time (BT), and (d) total ρR from a free-fall analysis of a 1 D Ares power scan with a square laser pulse (0.2 ns rise time, 0.1 ns fall time) incident on a 1.51 mm outer-diameter, 4.7 μm-wall SiO_2 capsule filled with 5.15 atm tritium, 0.05 atm deuterium, and 2.6 atm ^{3}He. Red squares represent 27 TW, green triangles 40 TW, purple x's 54 TW, blue diamonds 81 TW, cyan asterisks 108 TW, orange circles 135 TW, and gray crosses 162 TW absorbed laser power. The dashed red line in panel (c) indicates which part of parameter space gives bang-time before and after the end of the laser pulse, respectively (note that the rise time is included in the quoted pulse duration, while the fall time is not). The yellow stars approximately indicate the predictions for shot N161214–001 and the red stars the predictions for N161214–002 (assuming 61% absorption).

TABLE I. Parameters of three $T_2/^3$He-gas-filled thin-glass shell exploding pushers shot with varying laser drive.

Shot	Pulse shape	Pulse length (ns)	Laser energy (kJ)	Capsule diameter (μm)	Shell thickness (μm)	T2 fill pressure (atm)	^{3}He fill pressure (atm)	Initial density (mg/cm^3)
N160601-002	Ramp	2.1	111.3	1594	4.6	2.65	5.98	1.42
N161214-001	Square	1.7	101.2	1511	4.7	2.63	5.38	1.33
N161214-002	Square	1.3	176.0	1512	4.6	2.63	5.37	1.33

worthwhile goal. According to the simulations, extended pulse duration leads to increased T_{ion} and yield up to a power-dependent point. At further extended pulse duration, T_{ion} and yield then plateau, indicating that the laser pulse could be turned off early without detrimental impact on these parameters. (The yield saturates very rapidly with pulse duration for high absorbed laser power.)

Translating the simulated results to an experimental prediction requires an assumption about the fraction of incident laser power absorbed by the capsule. The established method for doing this is to use scattered light diagnostics to obtain a direct measurement of absorbed laser light fraction.[29] This works well for symmetric direct drive on the OMEGA laser, where backscattered light measurements in a few discrete detectors can be reliably extrapolated to a total absorbed fraction. While scattered light diagnostics are available also on the NIF,[30] the PDD geometry [Fig. 1(a)] means that sophisticated modeling is required to convert the discrete detector measurements to total absorbed light fraction. (Note also that even the best available modeling capabilities of laser-plasma interactions are non-predictive and very uncertain, especially at high power.) We assume an absorbed laser light fraction of 61% for these SiO_2-shell implosions based on the free-fall analysis of a 1 D-Ares energy scan for TT-filled reference NIF implosion N160530–001 (1.6 mm OD, 4.7–μm SiO2 shell, see Ref. 9), which found that measured bang time, yield, and T_{ion} were extremely well captured by the simulation for an absorbed laser light fraction of 61% (measured TT-n yield $(8.2\pm1.7)\times10^{11}$, simulated 8.4×10^{11}; measured bang time 2.05 ± 0.03 ns, simulated 2.06 ns; measured DT T_{ion} 8.2 ± 0.2 keV, simulated 8.1 keV). While this solution may well be non-unique, it is also in reasonable agreement with a pre-shot 2 D SAGE[31] calculation, which predicted an absorbed fraction of 68% for this experiment.

Experimentally, the impact of laser pulse shape on implosion performance is assessed by comparing the results from three nominally identical, $T_2/^3$He-gas-filled capsules (Table I) imploded with (i) a 2.1 ns, 111.3 kJ ramped laser pulse with 100 TW peak power (Ref. 9), (ii) a 1.7 ns, 60 TW, 101.2 kJ square laser pulse, and (iii) a 1.3 ns, 140 TW, 176 kJ square laser pulse. (The two square-pulse laser drives are indicated with stars in Fig. 3, assuming 61% absorption.) The laser pulse shapes are visualized in Fig. 4, along with the x-ray burn histories (or bang times) measured using the SPIDER diagnostic.[32] Table II summarizes the results from the three implosions. The 5–10 MeV TT-n yield, the DT-n yield, and the DT T_{ion} are measured using the nTOF Spec detectors.[33,34] The T^3He-d yield is measured using the magnetic recoil spectrometer[35] (MRS; note that only the statistical uncertainty is quoted, the systematic uncertainty is estimated to be ~20% in this charged-particle measurement due to possible fluence anisotropy around the implosion). The D^3He-p yield and mean energy ($E_{D3He\text{-}p}$) are weighted averages of 6–7 measurements[36] distributed around the implosion (see Fig. 6). The uncertainty quoted is the uncertainty in the weighted average, multiplied by χ^2_{red} for the hypothesis that the weighted average represents all measurements for the cases where $\chi^2_{red} > 1$. The deuterium impurity (which impacts DT and D^3He yields) is expected to be the same for N161214–001,002, which was filled at the same time, but much higher for N160601–002.

The first thing to note is that while ramped pulse shot N160601–002 was shot with 10% higher total energy than square pulse shot N161214–001, N161214–001 gave 6 ± 4% higher DT T_{ion}, 23 ± 22% higher TT yield, and 88 ± 28% higher T^3He-d yield, demonstrating better performance at lower laser energy for the square pulse shot. The second important observation is the substantial increase in T_{ion} and all measured yields when going from the low-power square pulse to the high-power square pulse. This difference was enough to generate a ^{3}He^{3}He-p spectrum with excellent statistics for a ^{3}He-gas-filled target shot with the higher-power square pulse, with a 5–11 MeV ^{3}He^{3}He-p yield of $(7.2\pm1.6)\times10^7$; this spectrum will be analyzed in detail in a future publication.

An all-important question in terms of using this platform to study the shape of charged-particle spectra such as ^{3}He^{3}He-p is whether charged particles escape the implosions undistorted. In Fig. 5, D^3He-proton and T^3He-deuteron spectra from the three shots are compared. The D^3He-p spectra represent an average of four measurements using wedge range filter (WRF) proton spectrometers[36] distributed around the equator of the implosion (at $\pm3.5°$ and $\pm13°$ from diagnostic insertion modules at polar-azimuthal angles of

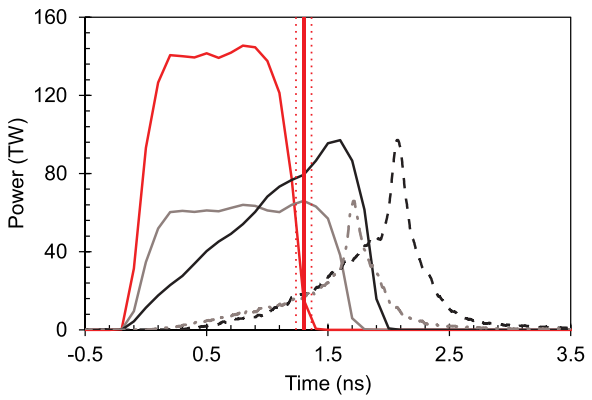

FIG. 4. As-shot laser power (absolute scale, solid lines) and x-ray burn history as measured using SPIDER (arbitrary scale, broken lines) for N160601–002 (ramped pulse, dashed burn history, black), N161214–001 (low-power square pulse, dashed-dot burn history, gray), and N161214–002 (high-power square pulse, red). SPIDER saturated for N161214-002. A bang time can be inferred from the data (red vertical line with dotted lines representing the error bar), but the absolute burn history is very uncertain and therefore not shown.

TABLE II. Results from the three T_2/^{3}He-gas-filled thin-glass-shell exploding pushers from Table I (see text for details). Note that the deuterium impurity content is substantially different for N160601-002 compared to N161214-001/002, which should be kept in mind when comparing DT and D^{3}He yields from the three implosions.

Shot	X-ray bang time (ns)	DT Tion (keV)	5–10 MeV TT-n yield ($\times 10^{10}$)	DT-n yield ($\times 10^{10}$)	MRS T^{3}He-d yield ($\times 10^9$)	D^{3}He-p yield ($\times 10^8$)	$E_{D3He\text{-}p}$ (MeV)
N160601-002	2.07 ± 0.03	7.8 ± 0.2	3.0 ± 0.6	21 ± 1	0.49 ± 0.01	2.7 ± 0.7	14.6 ± 0.9
N161214-001	1.69 ± 0.03	8.3 ± 0.2	3.7 ± 0.3	3.4 ± 0.1	0.92 ± 0.02	0.37 ± 0.05	14.5 ± 1.6
N161214-002	1.40 ± 0.04	12.5 ± 0.2	8.5 ± 0.7	7.2 ± 0.3	4.60 ± 0.03	2.8 ± 0.3	14.9 ± 0.5

90°–78° and 90°–315°, respectively); the T^{3}He-d spectra are measured using MRS at polar-azimuthal angles of 73°–324°. The nominal D^{3}He-p and T^{3}He-d birth energies are indicated by dashed vertical lines in Fig. 5. The spectra from low-power shots N160601–002 and N161214–001 are very clearly downshifted in energy compared to nominal and also show substantial deviation from the nominal Gaussian shape in the form of a low-energy tail (most likely due to ρR variation in time in this direction). Spectra from higher-power shot N161214–002 are much more symmetric in shape. Note that these spectra are slightly upshifted in energy relative to nominal; this is expected when the bang time happens right at the tail end of the laser pulse (compare Fig. 4). It is expected that truncating the higher-power laser pulse early, at 1.0 ns, would eliminate this problem without detrimental impact on yield (compare Fig. 3, which indicates that the pulse duration at this power setting could be reduced to 1.0 ns without losing yield).

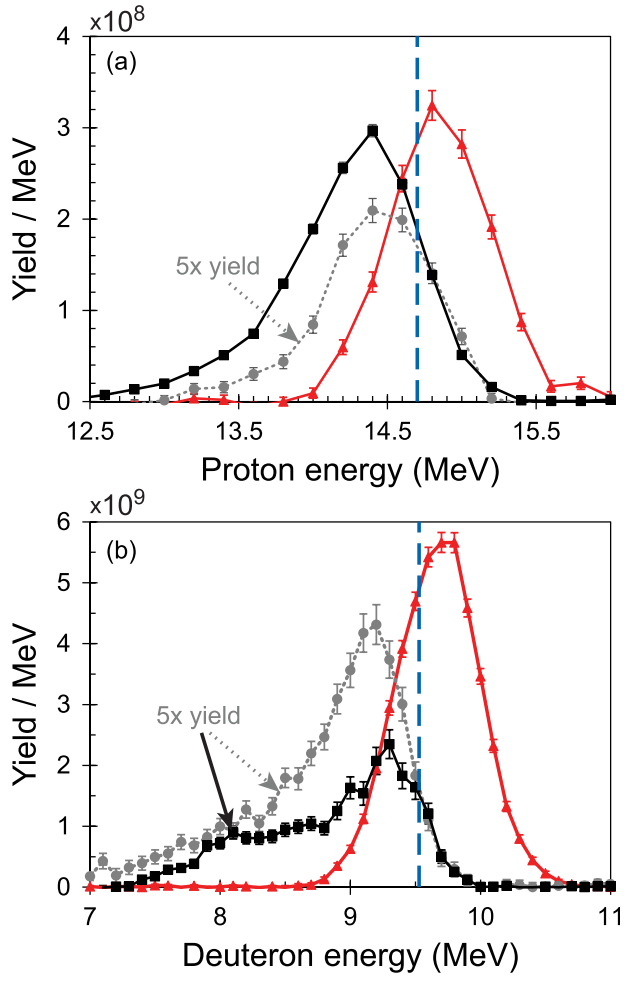

FIG. 5. (a) Average equatorial WRF D^{3}He-proton spectra and (b) MRS T^{3}He-deuteron spectra for shots N160601-002 (black squares), N161214-001 (gray circles, dotted line), and N161214–002 (red triangles). The D^{3}He-p yield for N161214-001 and the T^{3}He-d yields for N160601–002 and N161214–001 were multiplied by a factor of 5 to allow for easy comparison of the spectra. The vertical dashed lines indicate the nominal birth energy for D^{3}He-p (a) and T^{3}He-d (b), respectively.

In Fig. 6, mean D^{3}He-p energies and yields are shown versus position for all three shots (average values are summarized in Table II). Note that the deuterium impurity in the fuel is noticeably lower for shots N161214–001/002 than for shot N160601–002, leading to substantially lower D^{3}He-p yield for N161214–001 than for N160601–002. The uncertainty in the WRF analysis is larger for N161214–002 than for N160601–002 in spite of comparable yields; this is because of the higher T^{3}He-deuteron yield on N161214–002, which limits how long the CR-39 detectors used in the WRF spectrometers[37] can be etched without overlap issues. (N161214–002 data were etched for 1.5 h, N160601–002 data were etched for 3 h.) In principle, widths can be inferred from the measured spectra as well. Width numbers are not shown in Fig. 6 since the spectral width is not very meaningful for N160601–002 and N161214–001 due to large spectral distortions, and very uncertain for N161214–002 due to the short etch time.

From Fig. 6, we conclude that energies are more symmetric for the higher laser power implosion. The indication is that yields are more symmetric as well, but the large error bars on the N161214–002 data prevent any firm conclusions on this point. (Again, in order to avoid upshifts, we would need to truncate the laser pulse used on N161214–002. Bang after the end of the laser pulse is also expected to reduce yield variations around the implosion.[26]) In Fig. 7, x-ray images of the three implosions at bang time are compared. All shots show similar overall symmetry features, with relatively round images as viewed from the top (polar - azimuthal angles 0°–0°) and severely distorted images as viewed from the side (90°–78°). The better top-view symmetry is a natural consequence of the azimuthal drive symmetry in the PDD configuration [Fig. 1(a)]. N160601–002 and N161214–001 show a comparable shape, while the images from N161214–002 indicate slightly improved equatorial symmetry. Comparing N161214–001 and N161214–002 also indicates a larger core for the latter shot, presumably because of the faster shock propagation and burn in this case (compare Fig. 4), which means that the shell has not converged as far at the time of peak x-ray brightness (when the reflected shock interacts with the incoming shell). The improved symmetry and lower convergence are expected to contribute to

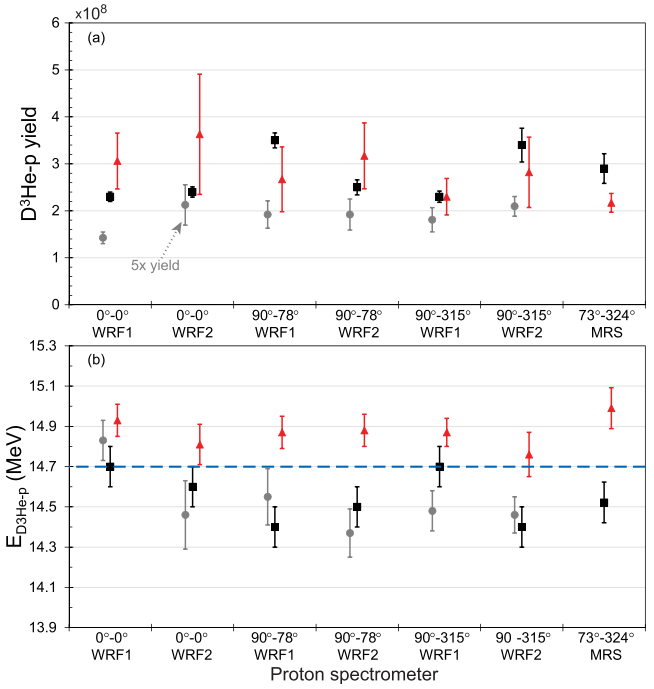

FIG. 6. (a) D^3He-p yields and (b) D^3He-p mean energies as measured using WRF proton spectrometers in six locations around the implosion and using the MRS. Black squares represent shot N160601–002, gray circles represent shot N161214–001 (the yield for this shot was multiplied by 5 to allow display on the same scale; MRS sensitivity is too low to allow measurement on this shot), and red triangles represent shot N161214–002. In panel (b), the nominal mean D^3He-p birth energy is also indicated (dashed blue line).

the lesser distortion in equatorial spectra observed from shot N161214–002 (compare Fig. 5), because of less mass accumulation in the equatorial direction.

While the comparison of results from N161214–001 and N161214–002 clearly shows that increasing the power from 60 to 140 TW leads to an increase in yield (Table II), the increase is smaller than predicted from the 1 D-Ares simulations (Fig. 3). In addition to the TT-n yields shown in Fig. 3, predicted D^3He-p, T^3He-d, and DT-n are also generated from the free-fall analysis of the Ares simulations. In Fig. 8, the measured yield amplifications between shots N161214–001 and N161214–002 are contrasted to the Ares-predicted yield amplifications, assuming 61% absorption.

The first question in making this comparison is whether it is reasonable to assume the same absorption fraction at the two power settings. While extrapolation of measurements of scattered light on the NIF to total absorbed light fraction is challenging due to the PDD geometry as discussed above, a relative scaling between two shots is straightforward to perform. Comparing the fast diode[30] scattered light measurements in four beams (#315–318) on shots N161214–001 and N161214–002 shows an average ratio of 1.70 times more scattered light for -002 (Table III), consistent with the 1.74 times higher laser energy delivered on that shot. This is consistent with the absorption being the same for both power settings.

There are many possible explanations for the observed differences in simulated and predicted yield amplification. While the assumption of the same relative absorption between the two power settings appears justified, the uncertainty in the absolute absorption is still large. Also, the simulations are 1 D, while we well know that the implosions are highly 2 D/3 D in nature (Fig. 7). The free-fall analysis applied to the simulation is also well known to be an approximation; there is a possibility that the alternative approach of using molecular diffusion multipliers might give better results (compare Ref. 6). The simulations do not consider ion-kinetic effects, which may also play a role for these implosions with a Knudsen number $N_k \sim 0.05$ (see Refs. 5,9; note that the dimensionless Knudsen number is calculated using the burn-averaged T_{ion} and is used to characterize a modified distribution function for the full ion population). While the simulations for the lower-power shot get T_{ion} approximately right, the simulations for the higher power shot substantially over-estimate T_{ion} (compare Fig. 3 and Table II). The simulated DT T_{ions} (not shown in Fig. 3) for the 81 TW simulation most closely describing shot N161214–002 are ~1.2 keV lower than simulated TT T_{ions}; this means that the simulations for the higher-power shot overestimate T_{ion} by more than a factor of 2. Given the stronger T_{ion}-dependence of the reactivity for D^3He and T^3He compared to DT and TT, this is also consistent with the significantly higher over-estimate of the yield amplification for the former two reactions than for the latter two. It is clear that while the 1 D simulation results presented in Fig. 3 are useful as a tool for predicting trends and guiding experimental design, they cannot be expected to be absolutely predictive for these implosions.

In summary, in this section it has been experimentally demonstrated that increasing the laser power used to implode thin-shell SiO_2 capsules leads to higher yields. The yield improvement is smaller than expected from 1 D-Ares simulations, likely because the simulations overestimate the increase in T_{ion} with power. 2 D/3 D effects and limited understanding of absorbed laser light fraction are expected to contribute to the differences observed between simulations and measurements. Charged particle spectra from the higher power shot are less distorted and more uniform around the implosion compared to spectra from the lower power shot, likely at least partially because of improved implosion symmetry. To fully optimize for charged-particle measurements, the laser pulse for the higher power shot should be truncated to 1.0 ns to avoid energy upshifts due to capsule charging; simulations indicate that this could be done without loss of yield. We have also demonstrated that using square pulses to implode thin-shell SiO_2 capsules gives higher yield at lower laser power compared to using a ramped pulse. While these results are very valuable for future diagnostic development and neutron source shots using this platform, what is really required for the nucleosynthesis platform is higher yield at lower T_{ion}. This motivates using larger capsules for these experiments (Sec. III).

III. USING LARGER CAPSULES

The square pulse power scan described in Sec. II demonstrated that sufficient yield to accurately probe the $^3He^3He$ reaction on the NIF could be achieved by imploding 1.6 mm-outer-diameter SiO_2 capsules with a square laser pulse, and that yield and T_{ion} increase with laser power. While this is a

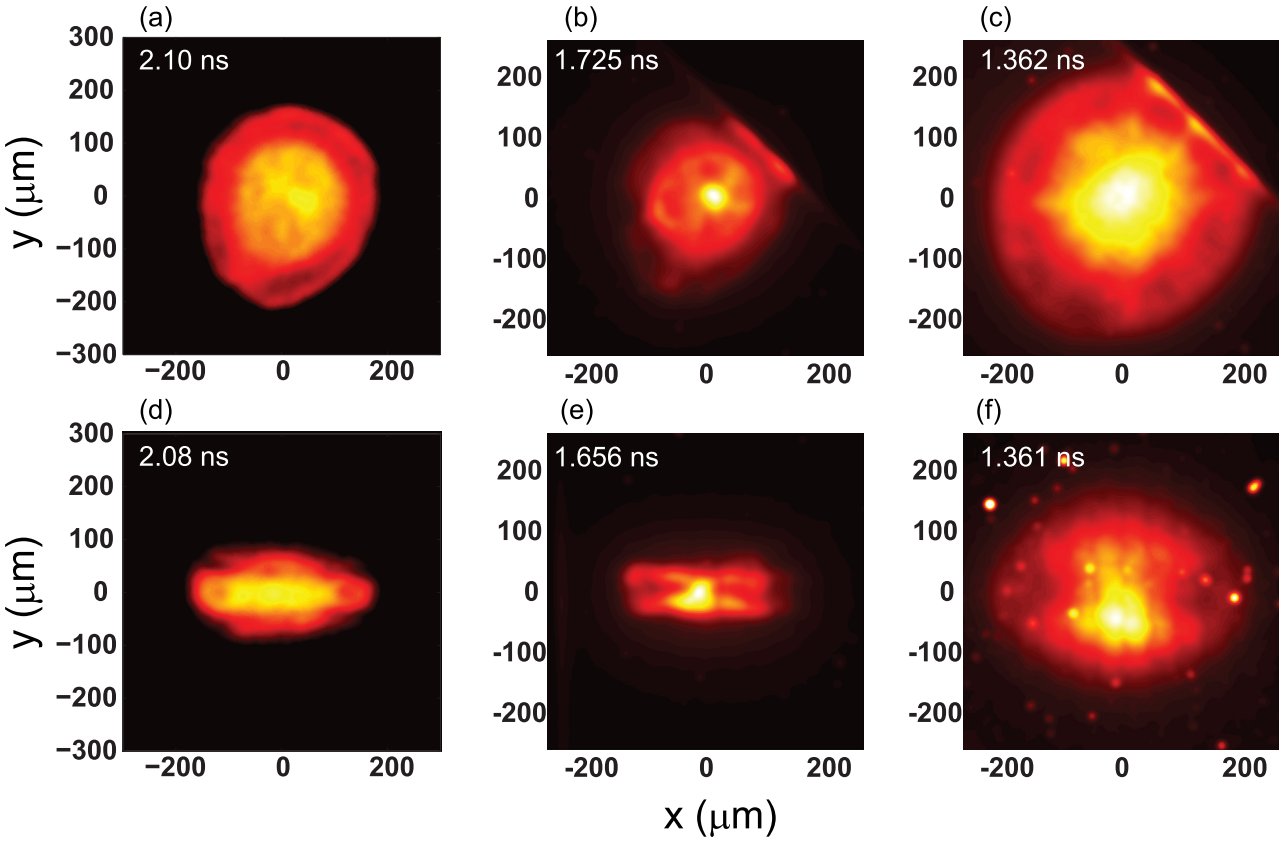

FIG. 7. X-ray images of the three T^3He implosions as viewed from (a)–(c) the top, at polar-azimuthal angles 0°–0°, and (d)–(f) the side, at polar-azimuthal angles 90°–78°. (a) and (d) Images are from shot N160601–002, (b) and (e) from shot N161214–001, and (c) and (f) from shot N161214-002. Note that while the color scale is directly comparable for N161214–001 and -002, the N160601–002 color scale is significantly different, which means that the relative size for this implosion cannot be inferred by looking at the images.

valuable result for other reasons, this type of high-T_{ion} implosion does not achieve conditions ideal for the study of stellar-nucleosynthesis-relevant reactions. The fusion reaction yield is proportional to (i) reactant densities, (ii) reactivity, which is a strong function of T_{ion}, (iii) burn volume, and (iv) burn duration. Hence, an obvious way to increase yield without increasing T_{ion} or areal density (which would cause charged particles to experience energy loss) is to increase the burn volume. This can be achieved on the NIF by imploding larger capsules using more laser energy.[38]

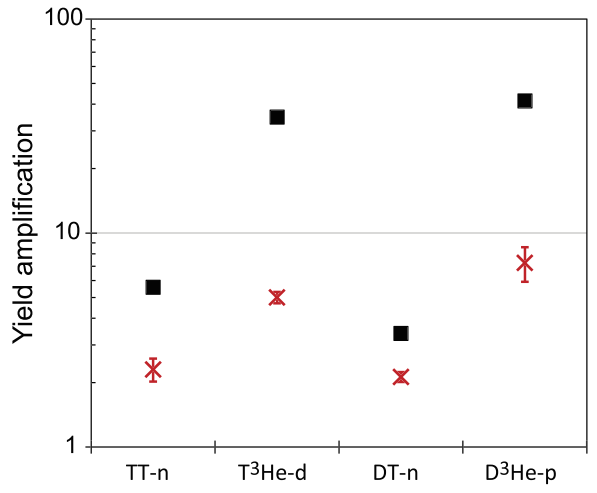

FIG. 8. Measured (red crosses) and simulated (black boxes) yield amplification when going from 60 to 140 TW delivered laser power (assuming 61% absorption for absorbed powers of 37 and 85 TW).

A platform to implode 3-mm OD, 18–μm-thick CH shell capsules using a 1.8-ns square pulse was recently developed with the initial goal of studying electron-ion equilibration.[6,7] The initial experiments using this platform, described in detail in Refs. 6,7, used D_2-gas-filled capsules and varied the fraction of laser energy delivered in the inner and outer laser beam cones [Fig. 1(a)] to tune implosion symmetry. In Fig. 9, the DD-neutron yields from this initial set of three 3-mm OD CH shell implosions (shots N160920–003, N160920–005, and N160921–001) are contrasted to the DD-neutron yield obtained from three D_2-gas-filled 1.6 mm-OD SiO_2 shell implosions equivalent to shot N160601–002 described in Sec. II (specifically, shots N101215–001, N120328–001,[5] and N130225–006). Interestingly, the comparison shows that the CH-shell implosions outperform the SiO_2-shell implosions by a higher fraction than expected from simple volume scaling. We note that the

TABLE III. Fast diode-measured scattered light in quad 31 on the NIF for shots N161214-001 and -002.

Beam	N161214-001 (J)	N161214-002 (J)	Ratio
B315	41.7	69.5	1.67
B316	25.6	46.9	1.83
B317	28.9	45.2	1.56
B318	55.4	96.6	1.74

measured T_{ions} are comparable or even a bit higher for the SiO_2 shells (8–11 keV) than for the CH shells (7.3–7.8 keV). The convergence ratios (CR) for the SiO_2 and CH shell implosions are also roughly equivalent,[39] and the initial fill pressures comparable at 10 atm for the SiO_2 shell case and 8 atm for the CH shell case, indicating similar number densities for the two cases (if anything, based on the higher initial fill pressure for the SiO_2-shell capsule, we may expect higher relative yield in this case). We conjecture that the improved symmetry for the larger capsules may be responsible for the additional boost in yield on top of the expected volume gain (compare Fig. 12; note that the symmetry is different for the three CH-shell implosions in Fig. 9 due to the varying cone fraction, but better than for the SiO_2-shell implosions in all cases). Reduced impact of ion-kinetic effects in the larger capsule implosions due to larger system scale size (hence lower Knudsen number) may also contribute to the improved performance.[5]

As an aside, it is also interesting to note that the energy used to drive the CH shell capsules from Fig. 9 is only 3.8 times higher than the energy used to drive the SiO_2 capsules, while the total mass of the CH capsules is ~5.5 times higher than the mass of the SiO_2 capsules. The fact that the laser energy increase is less than predicted by mass scaling[38] can be viewed as further evidence that the ramped laser pulse shape used to drive the SiO_2 shell implosions (equivalent to the laser pulse shape used for N160601–002; Fig. 4) is not optimized for high performance.

Clearly, the 3 mm-OD CH shell platform is an interesting possible path towards reaching the low T_{ion}, high yield goals for the nucleosynthesis studies. However, the initial CH-shell experiments did not address whether low enough ρR for accurate probing of charged-particle spectra could be achieved. A 1 D-Ares laser energy scan (Fig. 10) was performed as a first step towards addressing this question. The simulations were tuned to match the experimental results from the best-performing D_2-gas-filled 3 mm-OD shell implosion, N160920–005. The laser energy was then increased in two ways from this baseline, (i) by extending the laser pulse duration at fixed power (dashed lines, hollow symbols in Fig. 10), and (ii) by increasing the power at fixed pulse duration (solid lines/symbols in Fig. 10). The simulations show predicted total ρrs that are higher than the ideal <10 mg/cm^2 for charged-particle measurements. They also show that extending the laser pulse at fixed power is expected to lead to higher ρR, while increasing the power at fixed pulse duration should give minimally increased ρR.

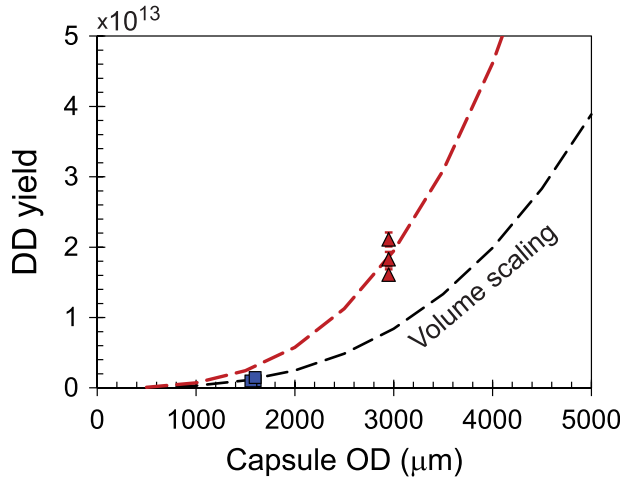

FIG. 9. DD neutron yield from six reference NIF exploding pusher implosions plotted as a function of capsule outer diameter (OD). The blue squares represent 1.6 mm-OD, 4.5-μm thick SiO_2 shells imploded using a ramped, 125 kJ laser pulse to give T_{ion} = 8–11 keV; the red triangles represent 3 mm-OD, 18-μm thick CH shells imploded using a square, 470 kJ laser pulse to give T_{ion} = 7.3–7.8 keV (Refs. 6,7). The dashed lines represent the yield increase expected as a function of capsule diameter if all other parameters (density, T_{ion}, burn duration) are kept the same.

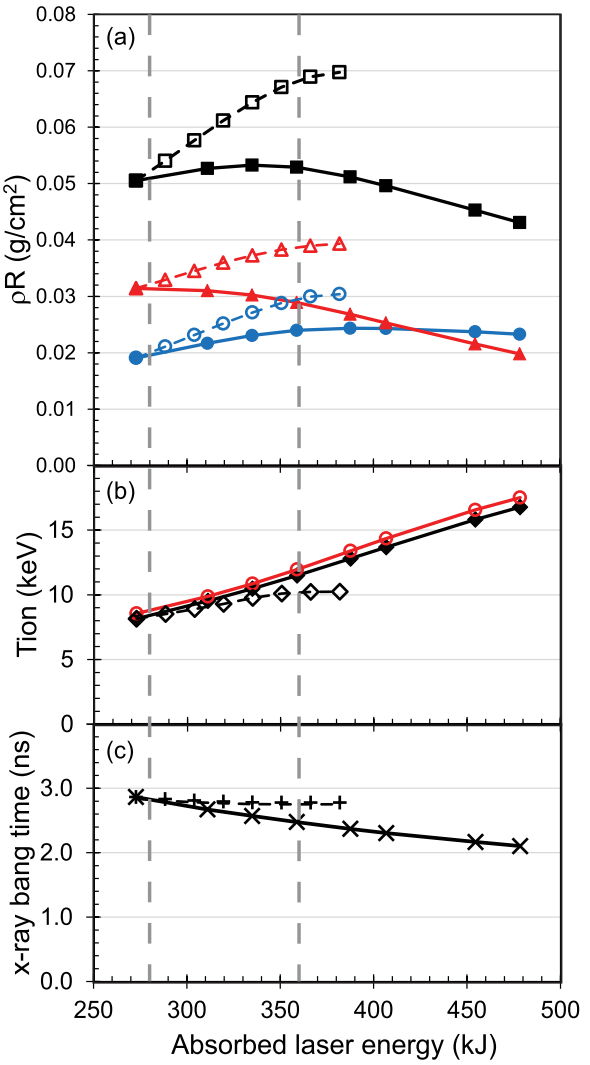

FIG. 10. Results from pre-shot 1 D Ares simulations tuned to match reference implosion N160920–005 shot with 470 kJ laser energy (left-most point, assumed total absorption 58%). Solid lines/symbols represent simulations scanning delivered laser power with pulse duration held fixed, dashed lines/hollow symbols simulations scanning pulse duration with delivered laser power held fixed. (a) Total ρR (black squares), shell ρR (red triangles), and fuel ρR (blue circles). (b) DD T_{ion} (black diamonds) and DT T_{ion} (red circles) from free-fall analysis. DT is only shown for the power scan. (c) x-ray bang time. The vertical dashed lines represent the best-estimate power settings (assuming 58% absorption) for N170212-003 (left) and -004 (right).

To experimentally test the value of this platform for ^{3}He^{3}He measurements, two initial ^{3}He-gas-filled implosions were performed, with parameters summarized in Table IV. These two implosions both used the same nominal pointing and cone fraction as reference implosion N160920–005. Different power settings were chosen for the two implosions as

TABLE IV. Parameters of the two ^{3}He-gas-filled CH shell exploding pushers shot with varying laser power.

Shot	Pulse shape	Pulse length (ns)	Laser energy (kJ)	Capsule diameter (μm)	Shell thickness (μm)	^{3}He fill pressure (atm)	Initial density (mg/cm^3)
N170212-003	Square	1.8	484	2950	17.6	10.2	1.28
N170212-004	Square	1.8	622	2956	18.0	10.2	1.28

TABLE V. Performance parameters for the two ^{3}He-gas-filled CH shell exploding pushers shot with varying laser power. Note that deuterium is present in these implosions as an impurity only; the deuterium content is not well quantified and is likely different for the two implosions, but is enough to give a strong D^{3}He-p signal in both cases.

Shot	X-ray bang time (ns)	X-ray burn duration (ps)	5–11 MeV ^{3}He^{3}He-p yield ($\times 10^8$)	D^{3}He-p yield ($\times 10^8$)	E_{D3He-p} (MeV)
N170212-003	2.99 ± 0.03	$423^{+24}/_{-18}$	0.40 ± 0.07	4.6 ± 0.2	14.19 ± 0.02
N170212-004	2.64 ± 0.04	$359^{+45}/_{-19}$	3.6 ± 0.3	5.9 ± 0.3	14.38 ± 0.02

a starting point for mapping out the optimal parameter space for high enough yield, low enough T_{ion} and low enough ρR. Note that eight laser beams[40] had to be dropped on both shots due to laser issues on shot day, so only 184 beams were used.

Results for the two implosions are summarized in Table V, and the laser pulse shapes and SPIDER-measured x-ray burn histories are illustrated in Fig. 11. The first thing to note is that the bang time change between the two shots (0.35 ns) almost exactly matches the expectation from the pre-shot power scan simulations (Fig. 10). The second thing to note is that bang-time falls well after the end of the laser pulse which, as discussed, is advantageous for charged-particle measurements.[26,27] The third thing to note is that while these capsules were fill-tube-filled with pure ^{3}He gas, a clear D^{3}He-proton signal is observed on both shots, indicating that a small deuterium impurity is present in the gas, likely due to residual deuterium in the fill plumbing.

Figure 12 shows top- and side-view self-emission x-ray images at bang time from the two implosions. Compared with the SiO_2-shell self-emission x-ray images in Fig. 7, these CH-shell images indicate significantly better symmetry as viewed from the side, which supports the hypothesis that improved symmetry may be responsible for larger-than-predicted performance improvements between the two implosion types (Fig. 9). Fits to the 30% of peak intensity contour of the equatorial x-ray images as a function of time for both shots were performed [an example fit is shown in Fig. 12(e)]. The average radii as a function of time inferred from these fits are shown in Fig. 12(f), which clearly shows how higher-power shot -004 implodes earlier and converges less than lower-power shot -003.

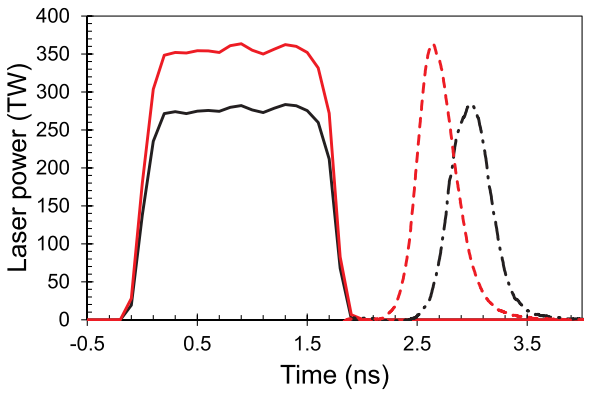

FIG. 11. Laser power (solid lines) and x-ray burn history (broken lines) for low-power CH shell shot N170212–003 (black, dash-dot burn history) and high power CH shell shot N170212-004 (red, dashed burn history).

The small residual deuterium impurity in the capsule fill is fortuitous as it allows us to address the usefulness of these implosions for charged-particle measurements. Eight WRF proton spectrometers were fielded on each of these implosions: four 50 cm from the target with a top view, and four 10 cm from the target with a side view. The top four WRFs were fielded at $\pm 13°/\pm 3.5°$ from the polar-azimuthal 0°–0° axis. The equatorial WRFs were fielded $\pm 21°$ in the equatorial plane from the polar-azimuthal 90°–78° and 90°–315° axes (since these WRFs are so close to the implosion, they span a broad range of angles from 7° to 36° from the axes). With D^{3}He-p yields of 5–6 $\times 10^8$ for these implosions (Table V), excellent D^{3}He-proton spectra were recorded on all eight detectors. The D^{3}He-p yields and mean energies (E_{D3He-p}) as well as the ^{3}He^{3}He yields quoted in Table V are weighted averages of the eight measurements. The uncertainties quoted are the uncertainties in the weighted average, multiplied by χ^2_{red} for the hypothesis that the weighted averages represent all measurements for the cases where $\chi^2_{red} > 1$.

D^{3}He-proton yields, mean energies, and spectral widths as measured with the eight individual detectors on the two shots are summarized in Fig. 13. The spectral widths are quoted as an upper limit on D^{3}He T_{ion}, inferred assuming the entire spectral broadening results from thermal Doppler broadening only ($\sigma = 76.681 \times \sqrt{T_{ion}}$ keV). Excellent uniformity is seen in the yields and mean energies from both shots [Figs. 13(a) and 13(b)]. The spectra for both shots are very clearly downshifted from the nominal 14.7 MeV birth energy with a mean energy of 14.19 MeV for shot N170212–003 and 14.32 MeV for shot N170212–004, providing evidence of remaining ρR at burn for both implosions. Excellent width uniformity [Fig. 13(c)] is seen for shot N170212–004. An average upper limit D^{3}He $T_{ion} = 16.7 \pm 0.4$ keV is inferred from all detectors for this shot. For shot N170212–003, the spectra as viewed from polar-azimuthal angles 90°–78° show substantially larger width (and more distortion) than spectra as viewed from other angles. The reason for this asymmetry is still under investigation, but one hypothesis is that it could be related to the eight dropped laser beams.[40] These

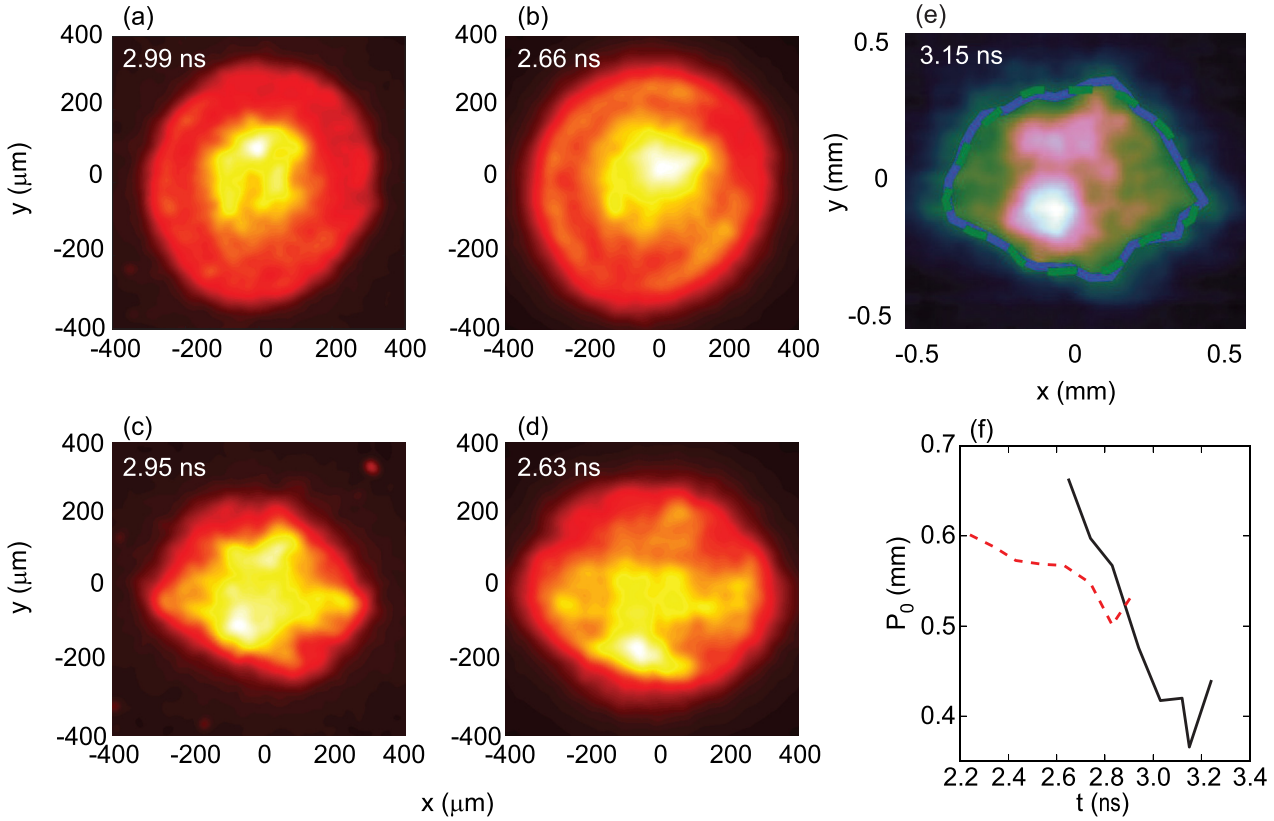

FIG. 12. Self-emission x-ray images at bang time as viewed from the pole [polar-azimuthal angles 0°–0°; (a) and (b)] and the equator [90°–78°; (c) and (d)] for shots N170212-003 (a) and (c) and N170212-004 (b) and (d), respectively. Panel (e) shows the equatorial x-ray image at t = 3.15 ns from shot N170212-003 including a fit to the 30% of peak intensity contour. This type of fit was used to infer the radius versus time for N170212-003 (solid black) and N170212-004 (dashed red) shown in panel (f).

eight laser beams are bundled around azimuthal angles 259° (upper four beams) and 191° (lower four beams), for an average azimuthal angle impacted of 225°. This is close to opposite in azimuthal angle to the WRFs at 90°–78° (the upper four beams are directly opposite), meaning that the implosion would be driven relatively harder in the 90°–78° direction, leading to more ρR. We conjecture that the effect is less obvious for N170212–004 due to the lower convergence and earlier implosion in this case [compare Fig. 12(f)]. Excluding the distorted 90°–78° data, an average upper limit D^3He $T_{ion} = 18.1 \pm 0.6$ keV is inferred for shot N170212–003. Note that these upper limit T_{ions} should not be viewed as approximations of the actual T_{ions} for these implosions; there will certainly be other broadening effects that also contribute to the spectral width, including broadening due to fuel ρR at burn (see further discussion below).

Figure 14 shows the average D^3He-p spectra from all WRFs except the two on 90°–78° for shot N170212–003, and from all eight WRFs for shot N170212–004. The average spectrum from N170212–003 shows a small but clearly evident low-energy tail and some skew relative to the nominally expected Gaussian shape. The average spectrum from N170212–004, on the other hand, is remarkably Gaussian over nearly three orders of magnitude in spite of the small downshift in energy relative to nominal. Excellent $^3He^3He$-p spectra were also measured on these shots but are not shown, as they will be the topic of an upcoming publication. Given that the noise floor in the D^3He-p measurement is about 3 orders of magnitude below the peak (Fig. 14), and the $^3He^3He$-p spectrum ~10 times wider than the D^3He-p spectrum, we roughly estimate that a $^3He^3He$-p yield more than $1/100^{th}$ of the D^3He-p yield is required for a strong measurement of the $^3He^3He$-p spectrum.

The observed spectral distortions are small enough that it is reasonable to think that we could accurately correct for them to report $^3He^3He$ birth spectra from these implosions. This is simplified by the fact that burn happens well after the end of the laser pulse (Fig. 11), which means no charged-particle energy upshifts due to capsule charging are expected. However, to properly correct the $^3He^3He$ spectra, we need to know the relative contribution of fuel and shell ρR. There is degeneracy between the broadening/downshift impact of fuel and shell ρR and Doppler broadening due to T_{ion} in the D^3He-p spectra. While fuel ρR gives rise to more broadening than shell ρR at an equivalent level, T_{ion} also gives rise to broadening, and many possible combinations of the three parameters can be invoked to explain the spectra in Fig. 14; in essence, the three parameters, T_{ion}, fuel, and shell ρR, cannot be uniquely constrained by the two observables, broadening and downshift. To fully constrain T_{ion} and fuel and shell ρR for these implosions, further information is required. This information could be obtained from an identical implosion with a higher deuterium content; enough to measure T_{ion} from the DD-neutron spectrum and fuel ρR from the ratio of secondary DT-n to primary DD-n yields.[41] Note that it is extremely important for the $^3He^3He$ work to

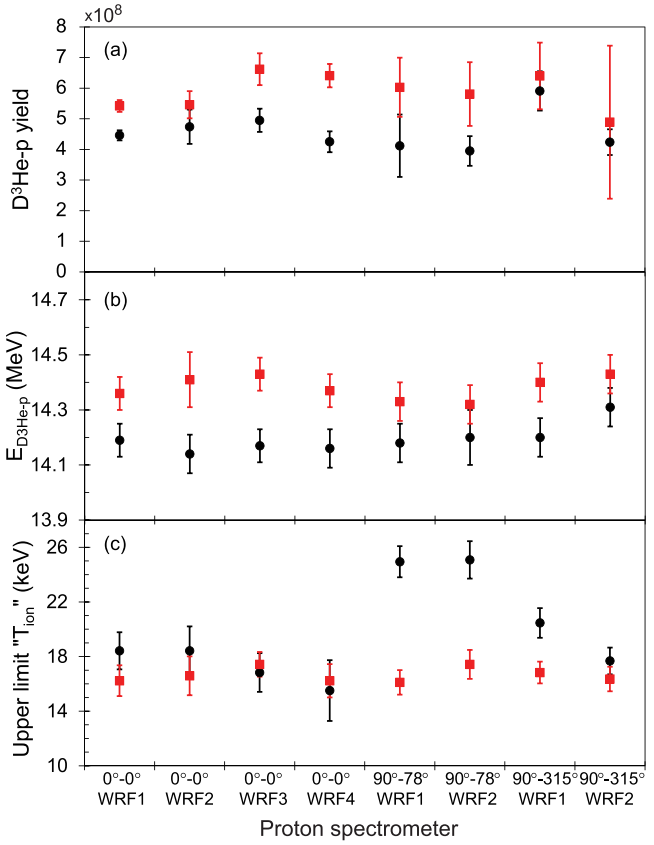

FIG. 13. D^3He-p (a) yield, (b) mean energy, and (c) spectral broadening as measured in eight different lines-of-sight on N170212-003 (black circles) and N170212-004 (red squares). The spectral broadening (c) is quoted as an upper limit on D^3He T_{ion}, inferred assuming the entire spectral broadening results from thermal Doppler broadening only.

know at what T_{ion} (hence center-of-mass energy[10]) we probe this reaction. (We know from Fig. 13 that T_{ion} from shot N170212–003 is no higher than 18 keV and T_{ion} from N170212–004 no higher than 17 keV. However, the true T_{ion} from these implosions is expected to be significantly lower than that, we roughly estimate ~8.5 keV for -003 and ~10.5 keV for -004 based on reactivity scaling[42] from N160920–005.)

It is instructive to compare the measured D^3He-p spectra with expectation based on simulations. Our two ^3He-gas-filled CH-shell shots have been simulated using the 1 D radiation hydrodynamics code NYM,[43] calibrated to reference D_2-gas-filled implosion N160920–005.[6] The top panels of Figs. 15 and 16 show NYM-simulated D^3He burn histories and burn-averaged D^3He T_{ion} as a function of time for shots N170212–003 (Fig. 15) and N170212–004 (Fig. 16). The timing of the NYM simulations is aligned to reproduce the measured x-ray bang time. Synthetic D^3He-p spectra have been generated using NYM-simulated radial profiles of T_{ion}, electron temperature (T_e), and density (ρ) at a few discrete times (indicated with data points in the upper panels of Figs. 15 and 16). These spectra are generated using a Monte Carlo model to (i) seed D^3He protons in spherical geometry, with properly weighted radial probabilities based on the T_{ion}/ρ profiles, and (ii) transport them to an imagined detector using Li-Petrasso stopping,[44] considering the ρ and T_e profiles. For reference, the fuel and shell ρRs inferred from the NYM profiles are also shown in the top panels of Figs.

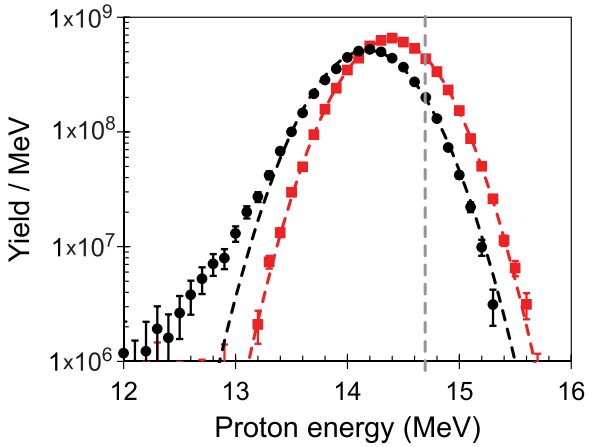

FIG. 14. Average D^3He-proton spectra from shots N170212-003 (black circles; the distorted 90°–78° data are excluded in the averaging) and N170212-004 (red squares). The vertical dashed line represents the nominal D^3He-p birth energy. Also shown are Gaussian fits to the spectra (dashed lines). The N170212-004 data are extremely well described by the Gaussian over nearly 3 orders of magnitude; for N170212-003, there is a tail towards low energy and a little bit of a skew.

15 and 16. The measured D^3He-p spectra (Fig. 14) are contrasted to synthetic spectra folded with the WRF instrument response in the lower panels of Figs. 15 and 16 (note that all spectra, synthetic and measured, are area normalized in this comparison). For lower-power shot N170212–003, the measured spectrum is rather well described by the synthetic spectrum at the earliest time studied (2.655 ns). However, this good match should not be viewed as evidence that we have found a unique solution. Synthetic spectra at later times are substantially more downshifted than the measured spectrum, which obviously means that the burn-averaged simulated spectrum will be significantly broader than the measured burn-averaged spectrum. For higher-power shot N170212–004, synthetic spectra at all times studied over-estimate the downshift. Broadening is also somewhat overestimated at the earliest time (assuming the entire broadening is due to T_{ion}, T_{ion} = 20 keV from the simulation vs T_{ion} = 17 keV from the measurement).

The synthetic spectra provide a quick reference for what the expected impact on the D^3He-p spectra is of various combinations of T_{ion} and fuel and shell ρR. The comparison to measured spectra leads to the conclusion that the dynamics of these implosions are important in the interpretation of results. The D^3He burn histories from the 1 D-NYM simulations are seen to be double-peaked. However, these are clean, 1 D simulations. Given the observed asymmetries for these implosions (Fig. 12) and potential mix, the second peak is not expected to survive intact (in fact, if fall-line analysis was applied to this simulation, it would almost entirely eliminate this peak). Still, the timing of the second peak provides a better match to observed x-ray bang time for these implosions. This is believed to be because the x-ray peak is generated by the outgoing shock colliding with the incoming shell, which happens at about the time of peak compression, responsible for the second burn peak in the simulation. If this hypothesis holds, we expect to see a significant difference between nuclear and x-ray bang times for these implosions. (Given the predicted strong variation of T_{ion} during burn [Fig. 15(a)], such a difference might be expected to be even larger for D^3He than for

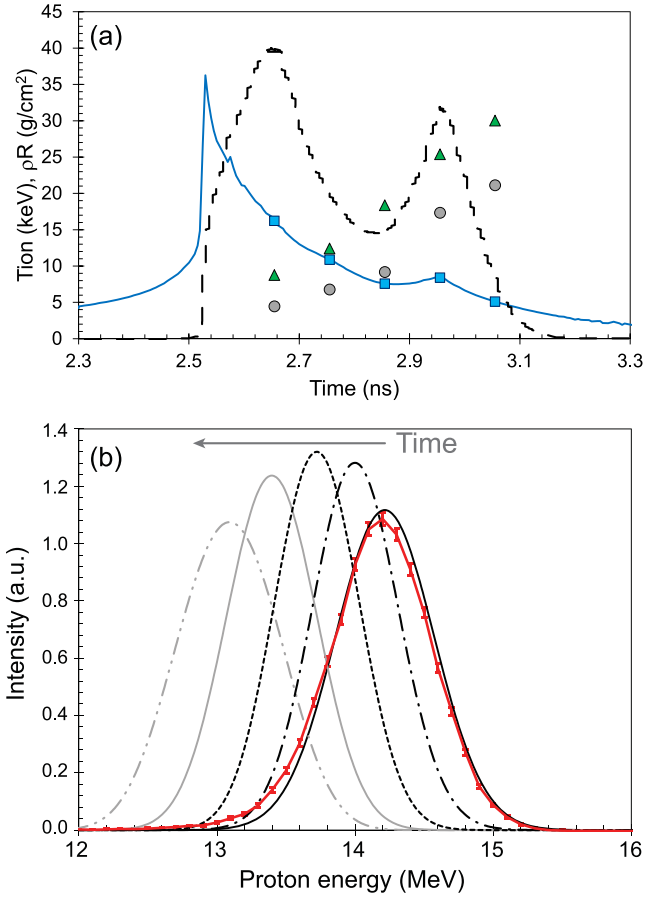

FIG. 15. (a) 1 D-NYM simulated D^3He-burn-weighted T_{ion} (solid line), D^3He burn history (dashed line, arbitrary units), fuel (circles), and shell (triangles) ρR for shot N170212–003 as a function of time. Fuel and shell ρRs are determined by post-processing NYM-simulated radial density profiles at the indicated five times. (b) Area-normalized synthetic D^3He-proton spectra generated using the NYM-simulated radial profiles at the times indicated in (a), folded with the WRF proton spectrometer response and contrasted to the measured spectrum for shot N170212-003 (red line with error bars).

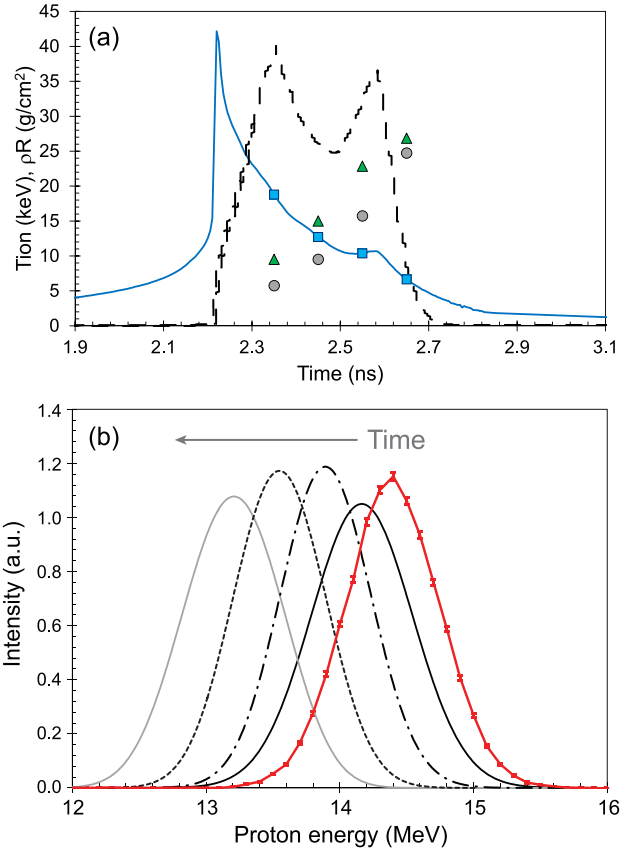

FIG. 16. Same as Fig. 15 but for shot N170212-004.

DD or DT, due to the different T_{ion} dependence of the reactivities[45] for these reactions.) The hypothesis that nuclear burn at late time is truncated relative to the 1 D prediction is supported by the fact that the D^3He-p spectra are best matched by the simulated ρR at early times. It is also supported by preliminary measurements of the D^3He bang time for these implosions using the MagPTOF diagnostic,[46] which indicate D^3He bang times of 2.6 ± 0.1 ns for shot N170212–003 and 2.1 ± 0.1 ns for shot N170212–004. The measured MagPTOF bang time for N170212–003 correlates nearly exactly with the first peak in the simulated burn history. Although for N170212–004 agreement of the measured MagPTOF with the synthetic burn history is less good, it still falls substantially ahead of the x-ray bang time. The difference in simulations and measurements in this case is not yet fully understood, but the early MagPTOF bang time suggests that nuclear yield is dominated by the initial shock and subsequent burn is even further truncated by deviations from 1 D behavior.

Kinetic effects such as tail ion depletion[47,48] have emerged as an important topic to be considered in connection with exploding pusher implosions.[5,9] As for the impact of tail ion depletion on our $^3He^3He$ work, the first thing to note is that this is not expected to impact the proton spectral measurements. Knudsen numbers for N170212–003 and -004 are crudely estimated to be 0.01 and 0.02, respectively, based on T_{ion} from reactivity scaling and burn region size from inspection of x-ray images. Using the fuel ion distribution as defined in terms of N_k by Albright *et al.*[48] we estimate a reactivity reduction relative to Maxwellian of 4% for $^3He^3He$ and 5% for D^3He at $N_k = 0.02$ and $T_{ion} = 10.5$ keV. As planned measurements of the reactivity of the $^3He^3He$ reaction will be made based on the ratio of $^3He^3He$-p to D^3He-p yields, an effect on this level would be negligible. However, the possible impact of kinetic effects on this work is a very important question, and we plan to follow up this initial analysis with more detailed simulations to thoroughly address this topic.

In summary, in this section it has been clearly demonstrated that larger capsules work for generating higher yield at equivalent T_{ion}. Improved symmetry with larger capsules when using polar-direct drive may contribute to higher yields. The 3 mm-OD capsules used in this work were driven with up to 0.62 MJ; this leaves room to drive even larger capsules using more of the available 1.8 MJ laser energy on the NIF to push these yields even further. From mass scaling, we expect that 1.1 MJ energy and 490 TW power would be required[38] to drive a 4 mm-OD capsule to equivalent conditions as for shot N170212–003. This would give a further factor 2.4 increase in yield at equivalent T_{ion}.

In terms of nucleosynthesis experiments, high enough $^3He^3He$ yield ($>10^7$) at an interesting T_{ion} (bridging the gap between the OMEGA measurement at $T_{ion} = 27$ keV and the center of the sun at $T_{ion} = 1.3$ keV) can be obtained from

these CH shell implosions. We have shown that emitted charged-particle spectra are (for the most part) uniform around the implosion, unaffected by upshifts due to capsule charging, and minimally distorted by remaining areal density at burn, but that improved understanding of the relative impact of fuel and shell ρR is required for accurate interpretation of the ^{3}He^{3}He data.

IV. CONCLUSIONS

Pulse shape optimization and capsule optimization have been pursued as avenues toward improving the NIF polar-direct-drive exploding pusher platform as a high-yield, low-areal-density fusion product source for nucleosynthesis experiments in a stellar-relevant environment.

From the pulse shape study, it is concluded that 1.6 mm-outer-diameter glass-shell capsules are more effectively driven with square than ramped laser pulses, with the same capsules generating higher yield and higher T_{ion} when driven with a square pulse of equivalent energy. Yield and T_{ion} from these capsules are also found to increase with increased laser power, albeit by less than predicted by 1 D simulations, and ρR is found to decrease with increased laser power. At 140 TW power, symmetric, minimally distorted charged-particle spectra are obtained from these implosions, although when shot with 1.3 ns pulse duration, the spectra are upshifted in energy due to capsule charging. Based on simulations, we expect that such upshifts could be avoided without loss of yield by truncating the laser pulse to 1.0 ns.

While the findings on improved implosion performance with square laser pulses and scaling of yield with power are expected to be important for various other campaigns utilizing this platform, the high values of T_{ion} resulting from these implosions are not ideal for studying stellar nucleosynthesis-relevant reactions. The capsule size study conclusively demonstrates, by comparing results from 1.6 and 3 mm-outer-diameter capsules, that higher yields at maintained T_{ion} can be obtained using larger targets. Excellent symmetry of emitted charged-particle spectra is also demonstrated for 3 mm-outer-diameter CH shell implosions. The ^{3}He^{3}He-p data from N170212–003 and N170212–004 are of high enough quality to be published. The spectra are downshifted in energy due to remaining areal density at burn, but at a low enough level that we expect to be able to accurately correct for it. As a next step, equivalent D^{3}He-gas-filled implosions will be executed, with a high enough deuterium content to accurately infer T_{ion} from the DD-neutron spectra and to measure secondary DT-neutron yield (the exact deuterium fraction required is still being determined). The secondary DT neutrons will be used to determine fuel ρR.[41] With T_{ion} and fuel ρR thus constrained, shell ρR can be obtained from the D^{3}He-proton spectra. D^{3}He-p core images will also be recorded to determine implosion size, from which density will be inferred. With this new information, accurate interpretation of already measured ^{3}He^{3}He-p spectra will be possible. Equivalent implosions with the minimum deuterium content that can be accurately characterized (low enough to allow measurement of ^{3}He^{3}He-p spectra) will then be executed in an attempt to directly measure the ^{3}He^{3}He reactivity from the ratio of ^{3}He^{3}He-p to D^{3}He-p yields. Finally, we would also like to push the platform to even larger capsules (4-mm targets) to make additional ^{3}He^{3}He measurements at even lower T_{ion}.

ACKNOWLEDGMENTS

The authors would like to thank the NIF operations crew for executing these experiments, and Ernie Doeg, Robert Frankel, and Michelle Valadez for processing of the CR-39 data used in this work. This material was based upon work supported by the Department of Energy, National Nuclear Security Administration under Award Nos. DE-NA0001857, DE-NA0002949, DE-NA0002905, DE-FG02–88ER40387, and DE-NA-0001808. Results from Nym simulations are (c) British Crown Owned Copyright 2018/AWE. This report was prepared as an account of work sponsored by an agency of the United States Government. Neither the United States Government nor any agency thereof, nor any of their employees, makes any warranty, express or implied, or assumes any legal liability or responsibility for the accuracy, completeness, or usefulness of any information, apparatus, product, or process disclosed, or represents that its use would not infringe privately owned rights. Reference herein to any specific commercial product, process, or service by trade name, trademark, manufacturer, or otherwise does not necessarily constitute or imply its endorsement, recommendation, or favoring by the United States Government or any agency thereof. The views and opinions of authors expressed herein do not necessarily state or reflect those of the United States Government or any agency thereof.

[1]B. M. Van Wonterghem, S. J. Brereton, R. F. Burr, P. Folta, D. L. Hardy, N. N. Jize, T. R. Kohut, T. A. Land, and B. T. Merritt, Fusion Sci. Technol. **69**, 452–469 (2016).
[2]S. LePape, A. Mackinnon, P. McKenty, S. Craxton, S. Janezic, T. Ma, R. Tommasini, P. Patel, N. Izumi, A. Nikroo, M. Hoppe, J. Caggiano, V. Glebov, J. Frenje, H. Herrmann, J. McNaney, G. Grim, R. Leeper, D. Bleuel, S. Friedriech, J. Knauer, R. Petrasso, H. Rinderknecht, C. Sangster, and J. D. Kilkenny, Bull. Am. Phys. Soc. **56**(12), 192 (2011).
[3]P. W. McKenty, R. S. Craxton, D. H. Froula, D. T. Michel, J. A. Marozas, T. C. Sangster, D. D. Meyerhofer, R. L. McCrory, J. D. Kilkenny, A. Nikroo, M. L. Hoppe, S. LePape, A. J. Mackinnon, and D. H. Munro, Am. Phys. Soc. **57**(12), 155 (2011).
[4]J. R. Rygg, A. B. Zylstra, F. H. Séguin, S. LePape, B. Bachmann, R. S. Craxton, E. M. Garcia, Y. Z. Kong, M. Gatu-Johnson, S. F. Khan, B. J. Lahmann, P. W. McKenty, R. D. Petrasso, H. G. Rinderknecht, M. J. Rosenberg, D. B. Sayre, and H. W. Sio, Rev. Sci. Instrum. **86**, 116104 (2015).
[5]M. J. Rosenberg, A. B. Zylstra, F. H. Séguin, H. G. Rinderknecht, J. A. Frenje, M. Gatu Johnson, H. Sio, C. J. Waugh, N. Sinenian, C. K. Li, R. D. Petrasso, P. W. McKenty, M. Hohenberger, P. B. Radha, J. A. Delettrez, V. Y. Glebov, R. Betti, V. N. Goncharov, J. P. Knauer, T. C. Sangster, S. LePape, A. J. Mackinnon, J. Pino, J. M. McNaney, J. R. Rygg, P. A. Amendt, C. Bellei, L. R. Benedetti, L. Berzak-Hopkins, R. M. Bionta, D. T. Casey, L. Divol, M. J. Edwards, S. Glenn, S. H. Glenzer, D. G. Hicks, J. R. Kimbrough, O. L. Landen, J. D. Lindl, T. Ma, A. MacPhee, N. B. Meezan, J. D. Moody, M. J. Moran, H.-S. Park, B. A. Remington, H. Robey, M. D. Rosen, S. C. Wilks, R. A. Zacharias, H. W. Herrmann, N. M. Hoffman, G. A. Kyrala, R. J. Leeper, R. E. Olson, J. D. Kilkenny, and A. Nikroo, Phys. Plasmas **21**, 122712 (2014).
[6]C. L. Ellison, H. D. Whitley, C. R. D. Brown, W. Garbett, H. Le, M. B. Schneider, Z. B. Walters, H. Chen, J. I. Castor, R. S. Craxton, M. Gatu Johnson, E. M. Garcia, F. R. Graziani, J. C. Hayes, G. E. Kemp, C. M. Krauland, P. W. McKenty, B. Lahmann, J. E. Pino, M. S. Rubery, H. A. Scott, and R. Shepherd, "Development and modeling of a polar direct drive exploding pusher platform at the National Ignition Facility," Phys. Plasmas (submitted).

[7]Z. B. Walters, H. D. Whitley, C. L. Ellison, W. Garbett, H. Le, H. Chen, C. Brown, J. I. Castor, S. Copeland, R. S. Craxton, M. Gatu Johnson, E. Garcia, F. R. Graziani, J. Hayes, G. E. Kemp, C. Krauland, P. McKenty, B. Lahmann, J. E. Pino, M. B. Schneider, H. A. Scott, R. Shepherd *et al.*, "Post-shot modeling of a polar direct drive platform on the National Ignition Facility," Phys. Plasmas (unpublished).

[8]D. T. Casey, D. B. Sayre, C. R. Brune, V. A. Smalyuk, C. R. Weber, R. E. Tipton, J. E. Pino, G. P. Grim, B. A. Remington, D. Dearborn, L. R. Benedetti, J. A. Frenje, M. Gatu-Johnson, R. Hatarik, N. Izumi, J. M. McNaney, T. Ma, G. A. Kyrala, S. MacLaren, J. Salmonson, S. F. Khan, A. Pak, L. Berzak Hopkins, S. LePape, B. K. Spears, N. B. Meezan, L. Divol, C. B. Yeamans, J. A. Caggiano, D. P. McNabb, D. M. Holunga, M. Chiarappa-Zucca, T. R. Kohut, and T. G. Parham, "Thermonuclear reactions probed at stellar-core conditions with laser-based inertial-confinement fusion," Nat. Phys. **13**, 1227 (2017).

[9]M. Gatu Johnson, A. B. Zylstra, A. Bacher, C. R. Brune, D. T. Casey, C. Forrest, H. W. Herrmann, M. Hohenberger, D. B. Sayre, R. M. Bionta, J.-L. Bourgade, J. A. Caggiano, C. Cerjan, R. S. Craxton, D. Dearborn, M. Farrell, J. A. Frenje, E. M. Garcia, V. Y. Glebov, G. Hale, E. P. Hartouni, R. Hatarik, M. Hohensee, D. M. Holunga, M. Hoppe, R. Janezic, S. F. Khan, J. D. Kilkenny, Y. H. Kim, J. P. Knauer, T. R. Kohut, B. Lahmann, O. Landoas, C. K. Li, F. J. Marshall, L. Masse, A. McEvoy, P. McKenty, D. P. McNabb, A. Nikroo, T. G. Parham, M. Paris, R. D. Petrasso, J. Pino, P. B. Radha, B. Remington, H. G. Rinderknecht, H. Robey, M. J. Rosenberg, B. Rosse, M. Rubery, T. C. Sangster, J. Sanchez, M. Schmitt, M. Schoff, F. H. Séguin, W. Seka, H. Sio, C. Stoeckl, and B. Tipton, Phys. Plasmas **24**, 041407 (2017).

[10]C. Iliadis, *Nuclear Physics of Stars: Second, Revised and Enlarged Edition* (Wiley-VCH Verlag GmbH & Co, Germany, 2015).

[11]A. B. Zylstra, J. A. Frenje, M. Gatu Johnson, G. M. Hale, C. R. Brune, A. Bacher, D. T. Casey, C. K. Li, D. McNabb, M. Paris, R. D. Petrasso, T. C. Sangster, D. B. Sayre, and F. H. Séguin, "Proton spectra from ^{3}He+T and ^{3}He+^{3}He fusion at low center-of-mass energy, with potential implications for solar fusion cross sections," Phys. Rev. Lett. **119**, 222701 (2017).

[12]A. B. Zylstra, H. W. Herrmann, M. Gatu Johnson, Y. H. Kim, J. A. Frenje, G. Hale, C. K. Li, M. Rubery, M. Paris, A. Bacher, C. Brune, C. Forrest, V. Glebov, R. Janezic, D. McNabb, A. Nikroo, J. Pino, T. C. Sangster, F. H. Séguin, W. Seka, H. Sio, C. Stoeckl, and R. D. Petrasso, Phys. Rev. Lett. **117**, 035002 (2016).

[13]T. R. Boehly, D. L. Brown, R. S. Craxton, R. L. Keck, J. P. Knauer, J. H. Kelly, T. J. Kessler, S. A. Kumpan, S. J. Loucks, S. A. Letzring, F. J. Marshall, R. L. McCrory, S. F. B. Morse, W. Seka, J. M. Soures, and C. P. Verdon, Opt. Commun. **133**, 495 (1997).

[14]E. G. Adelberger, A. Garcia, R. G. Hamish Robertson, K. A. Snover, A. B. Balantekin, K. Heeger, M. J. Ramsey-Musolf, D. Bemmerer, A. Junghaus, C. A. Bertulani *et al.*, Rev. Mod. Phys. **83**, 195 (2011).

[15]R. Bonetti, C. Broggini, L. Campajola, P. Corvisiero, A. D'Alessandro, M. Dessalvi, A. D'Onofrio, A. Fubini, G. Gervino, L. Gialanella, U. Greife *et al.*, Phys. Rev. Lett. **82**, 5205 (1999).

[16]M. Junker, A. D'Alessandro, S. Zavatarelli, C. Arpesella, E. Bellotti, C. Broggini, P. Corvisiero, G. Fiorentini, A. Fubini, G. Gervino, U. Greife, C. Gustavino, J. Lambert, P. Prati, W. S. Rodney, C. Rolfs, F. Strieder, H. P. Trautwetter, and D. Zahnow, Phys. Rev. C **57**, 2700 (1998).

[17]M. Gatu Johnson, C. J. Forrest, D. B. Sayre, A. Bacher, J.-L. Bourgade, C. R. Brune, J. A. Caggiano, D. T. Casey, J. A. Frenje, V. Y. Glebov, R. Hatarik, H. W. Herrmann, R. Janezic, Y. H. Kim, J. P. Knauer, O. Landoas, D. P. McNabb, R. D. Petrasso, J. E. Pino, B. Rosse, J. Sanchez, T. C. Sangster, H. Sio, W. Shmayda, C. Stoeckl, and A. B. Zylstra, "Observation of energy dependence in the T(t,2n)α neutron energy spectrum at center-of-mass energies in the range 16-50 keV," Phys. Rev. Lett. (submitted).

[18]S. Skupsky, J. A. Marozas, R. S. Craxton, R. Betti, T. J. B. Collins, J. A. Delettrez, V. N. Goncharov, P. W. McKenty, P. B. Radha, T. R. Boehly, J. P. Knauer, F. J. Marshall, D. R. Harding, J. D. Kilkenny, D. D. Meyerhofer, T. C. Sangster, and R. L. McCrory, Phys. Plasmas **11**, 2763 (2004).

[19]M. Hohenberger, P. B. Radha, J. F. Myatt, S. LePape, J. A. Marozas, F. J. Marshall, D. T. Michel, S. P. Regan, W. Seka, A. Shvydky, T. C. Sangster, J. W. Bates, R. Betti, T. R. Boehly, M. J. Bonino, D. T. Casey, T. J. B. Collins, R. S. Craxton, J. A. Delettrez, D. H. Edgell, R. Epstein, G. Fiksel, P. Fitzsimmons, J. A. Frenje, D. H. Froula, V. N. Goncharov, D. R. Harding, D. H. Kalantar, M. Karasik, T. J. Kessler, J. D. Kilkenny, J. P. Knauer, C. Kurz, M. Lafon, K. N. LaFortune, B. J. MacGowan, A. J. Mackinnon, A. G. MacPhee, R. L. McCrory, P. W. McKenty, J. F. Meeker, D. D. Meyerhofer, S. R. Nagel, A. Nikroo, S. Obenschain, R. D. Petrasso, J. E. Ralph, H. G. Rinderknecht, M. J. Rosenberg, A. J. Schmitt, R. J. Wallace, J. Weaver, C. Widmayer, S. Skupsky, A. A. Solodov, C. Stoeckl, B. Yaakobi, and J. D. Zuegel, Phys. Plasmas **22**, 056308 (2015).

[20]P. B. Radha, M. Hohenberger, D. H. Edgell, J. A. Marozas, F. J. Marshall, D. T. Michel, M. J. Rosenberg, W. Seka, A. Shvydky, T. R. Boehly, T. J. B. Collins, E. M. Campbell, R. S. Craxton, J. A. Delettrez, S. N. Dixit, J. A. Frenje, D. H. Froula, V. N. Goncharov, S. X. Hu, J. P. Knauer, R. L. McCrory, P. W. McKenty, D. D. Meyerhofer, J. Moody, J. F. Myatt, R. D. Petrasso, S. P. Regan, T. C. Sangster, H. Sio, S. Skupsky, and A. Zylstra, Phys. Plasmas **23**, 056305 (2016).

[21]R. M. Darlington, T. L. McAbee, and G. Rodrigue, Comput. Phys. Commun. **135**(1), 58 (2001).

[22]B. E. Morgan and J. A. Greenough, Shock Waves **26**, 355 (2016).

[23]M. M. Marinak, G. D. Kerbel, N. A. Gentile, O. Jones, D. Munro, S. Pollaine, T. R. Dittrich, and S. W. Haan, Phys. Plasmas **8**, 2275 (2001).

[24]Ares does not calculate absorption; an assumption has to be made in the simulation.

[25]L. Welser-Sherrill, J. H. Cooley, D. A. Haynes, D. C. Wilson, M. E. Sherrill, R. C. Mancini, and R. Tommassini, Phys. Plasmas **15**, 072702 (2008).

[26]C. J. Waugh, M. J. Rosenberg, A. B. Zylstra, J. A. Frenje, F. H. Séguin, R. D. Petrasso, V. Yu. Glebov, T. C. Sangster, and C. Stoeckl, Rev. Sci. Instrum. **86**, 053506 (2015).

[27]D. G. Hicks, C. K. Li, F. H. Séguin, A. K. Ram, J. A. Frenje, R. D. Petrasso, J. M. Soures, V. Y. Glebov, D. D. Meyerhofer, S. Roberts, C. Sorce, C. Stöckl, T. C. Sangster, and T. W. Phillips, Phys. Plasmas **7**, 5106 (2000).

[28]N. Sinenian, M. J.-E. Manuel, J. A. Frenje, F. H. Séguin, C. K. Li, and R. D. Petrasso, Plasma Phys. Controlled Fusion **55**, 045001 (2013).

[29]W. Seka, H. A. Baldis, J. Fuchs, S. P. Regan, D. D. Meyerhofer, C. Stoeckl, B. Yaakobi, R. S. Craxton, and R. W. Short, Phys. Rev. Lett. **89**, 175002 (2002).

[30]D. E. Bower, T. J. McCarville, S. S. Alvarez, L. E. Ault, M. D. Brown, M. P. Chrisp, C. M. Damian, W. J. DeHope, D. H. Froula, S. H. Glenzer, S. E. Grace, K. Gu, F. R. Holdener, C. K. Huffer, J. H. Kamperschroer, T. M. Kelleher, J. R. Kimbrough, R. Kirkwood, D. W. Kurita, A. P. Lee, F. D. Lee, I. T. Lewis, F. J. Lopez, B. J. MacGowan, M. W. Poole, M. A. Rhodes, M. B. Schneider, N. R. Sewall, F. Y. Shimamoto, S. J. Shiromizu, D. Voloshin, A. L. Warrick, C. R. Wendland, and B. K. Young, Rev. Sci. Instrum. **75**, 4177 (2004); J. D. Moody, P. Datte, K. Krauter, E. Bond, P. A. Michel, S. H. Glenzer, L. Divol, C. Niemann, L. Suter, N. Meezan, B. J. MacGowan, R. Hibbard, R. London, J. Kilkenny, R. Wallace, J. L. Kline, K. Knittel, G. Frieders, B. Golick, G. Ross, K. Widmann, J. Jackson, S. Vernon, and T. Clancy, Rev. Sci. Instrum. **81**, 10D921 (2010). P. Datte, A. M. Manuel, M. Eckart, M. Jackson, H. Khater, and M. Newton, "Target diagnostics physics and engineering for inertial confinement fusion II," Proc. SPIE **8850**, 885003 (2013).

[31]R. S. Craxton and R. L. McCrory, J. Appl. Phys. **56**, 108 (1984).

[32]S. F. Khan, P. M. Bell, D. K. Bradley, S. R. Burns, J. R. Celeste, L. S. Dauffy, M. J. Eckart, M. A. Gerhard, C. Hagmann, D. I. Headley, J. P. Holder, N. Izumi, M. C. Jones, J. W. Kellogg, H. Y. Khater, J. G. Kimbrough, A. G. MacPhee, Y. P. Opachich, N. E. Palmer, R. B. Petre, J. L. Porter, R. T. Shelton, T. L. Thomas, and J. B. Worden, Proc. SPIE **8505**, 850505 (2012).

[33]T. J. Clancy, J. Caggiano, J. McNaney, M. Eckart, M. Moran, V. Y. Glebov, J. Knauer, R. Hatarik, S. Friedrich, R. Zacharias, A. Carpenter, M. J. Shoup III, T. Buczek, M. Yeoman, Z. Zeid, N. Zaitseva, B. Talison, J. Worden, B. Rice, T. Duffy, A. Pruyne, and K. Marshall, SPIE Proc. **9211**, 92110A (2014).

[34]R. Hatarik, D. B. Sayre, J. A. Caggiano, T. Phillips, M. J. Eckart, E. J. Bond, C. Cerjan, G. P. Grim, E. P. Hartouni, J. P. Knauer, J. M. Mcnaney, and D. H. Munro, J. Appl. Phys. **118**, 184502 (2015).

[35]D. T. Casey, J. A. Frenje, M. Gatu Johnson, F. H. Séguin, C. K. Li, R. D. Petrasso, V. Y. Glebov, J. Katz, J. Magoon, D. D. Meyerhofer, T. C. Sangster, M. Shoup, J. Ulreich, R. C. Ashabranner, R. M. Bionta, A. C. Carpenter, B. Felker, H. Y. Khater, S. LePape, A. MacKinnon, M. A. McKernan, M. Moran, J. R. Rygg, M. F. Yeoman, R. Zacharias, R. J. Leeper, K. Fletcher, M. Farrell, D. Jasion, J. Kilkenny, and R. Paguio, Rev. Sci. Instrum. **84**, 043506 (2013).

[36]A. B. Zylstra, J. A. Frenje, F. H. Séguin, M. J. Rosenberg, H. G. Rinderknecht, M. G. Johnson, D. T. Casey, N. Sinenian, M. J.-E. Manuel, C. J. Waugh, H. W. Sio, C. K. Li, R. D. Petrasso, S. Friedrich, K. Knittel, R. Bionta, M. McKernan, D. Callahan, G. W. Collins, E. Dewald, T.

Döppner, M. J. Edwards, S. Glenzer, D. G. Hicks, O. L. Landen, R. London, A. Mackinnon, N. Meezan, R. R. Prasad, J. Ralph, M. Richardson, J. R. Rygg, S. Sepke, S. Weber, R. Zacharias, E. Moses, J. Kilkenny, A. Nikroo, T. C. Sangster, V. Glebov, C. Stoeckl, R. Olson, R. J. Leeper, J. Kline, G. Kyrala, and D. Wilson, Rev. Sci. Instrum. **83**, 10D901 (2012).

[37]F. H. Seǵuin, J. A. Frenje, C. K. Li, D. G. Hicks, S. Kurebayashi, J. R. Rygg, B.-E. Schwartz, R. D. Petrasso, S. Roberts, J. M. Soures, D. D. Meyerhofer, T. C. Sangster, J. P. Knauer, C. Sorce, V. Y. Glebov, C. Stoeckl, T. W. Phillips, R. J. Leeper, K. Fletcher, and S. Padalino, Rev. Sci. Instrum. **74**, 975 (2003).

[38]A. M. Cok, R. S. Craxton, and P. W. McKenty, Phys. Plasmas **15**, 082705 (2008).

[39]For SiO_2 shell implosion N120328, CR∼4.3 is inferred from the 17% contour of the x-ray image at bang time[5], while for N170212-003, which is nominally identical to N160920-005, CR∼4 is inferred from the 30% contour [see Fig. 12(f)]. However, this should be viewed as indicative only; caveats in this comparison are that the cameras may have been filtered differently on the two shots and that SiO_2 vs CH shells give rise to different x-ray signatures. In addition, 1D LILAC simulations for 2.1 ns ramped pulse implosions of 1.6 mm OD SiO_2 capsules as well as 1D Ares simulations of 1.8 ns square pulse implosions of 3 mm OD CH shell capsules each predict maximum CR∼11, based on minimum fuel-shell interface location.

[40]Q33 top and bottom were dropped. The as-shot inner/total cone fraction was 26% for both shots.

[41]H. G. Rinderknecht, M. J. Rosenberg, A. B. Zylstra, B. Lahmann, F. H. Séguin, J. A. Frenje, C. K. Li, M. Gatu Johnson, R. D. Petrasso, L. F. Brezak-Hopkins, J. A. Caggiano, L. Divol, E. P. Hartouni, R. Hatarik, S. P. Hatchett, S. LePape, A. J. Mackinnon, J. M. McNaney, N. B. Meezan, M. J. Moran, P. A. Bradley, J. L. Kline, N. S. Krasheninnikova, G. A. Kyrala, T. J. Murphy, M. J. Schmitt, I. L. Tregillis, S. H. Batha, J. P. Knauer, and J. D. Kilkenny, Phys. Plasmas **22**, 082709 (2015).

[42]The reactivity scaling uses the measured DD-n yield and T_{ion} from shot N160920-005 and, assuming equivalent burn profiles/dynamics for N160920-005 and N170212-003/004 but correcting for the small differences in initial densities, determines what T_{ion} from N170212-003/004 would have been based on measured $^3He^3He$ yield.

[43]P. D. Roberts, S. J. Rose, P. C. Thomson, and R. J. Wright, J. Phys. D: Appl. Phys. **13**, 1957 (1980).

[44]C. K. Li and R. D. Petrasso, Phys. Rev. Lett. **70**, 3059 (1993).

[45]H.-S. Bosch and G. M. Hale, Nucl. Fusion **32**, 611 (1992).

[46]H. G. Rinderknecht, H. Sio, J. A. Frenje, J. Magoon, A. Agliata, M. Shoup, S. Ayers, C. G. Bailey, M. Gatu Johnson, A. B. Zylstra, N. Sinenian, M. J. Rosenberg, C. K. Li, F. H. Sèguin, R. D. Petrasso, J. R. Rygg, J. R. Kimbrough, A. Mackinnon, P. Bell, R. Bionta, T. Clancy, R. Zacharias, A. House, T. Döppner, H. S. Park, S. LePape, O. Landen, N. Meezan, H. Robey, V. U. Glebov, M. Hohenberger, C. Stoeckl, T. C. Sangster, C. Li, J. Parat, R. Olson, J. Kline, and J. Kilkenny, Rev. Sci. Instrum. **85**, 11D901 (2014).

[47]K. Molvig, N. M. Hoffman, B. J. Albright, E. M. Nelson, and R. B. Webster, Phys. Rev. Lett. **109**, 095001 (2012).

[48]B. J. Albright, K. Molvig, C.-K. Huang, A. N. Simakov, E. S. Dodd, N. M. Hoffman, G. Kagan, and P. F. Schmit, Phys. Plasmas **20**, 122705 (2013).